

國立交通大學

電子物理研究所

碩士論文

Thermal fluctuations and disorder in

2D Ginzburg-Landau model



研究生：林宏燁

指導教授：儒森斯坦 教授

中華民國九十六年十月

Thermal fluctuations and disorder in 2D Ginzburg-Landau model

研究生：林宏燁

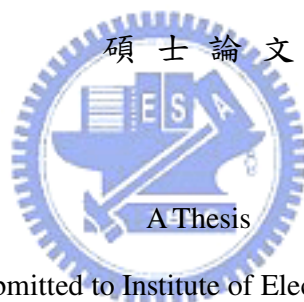
Student : Hung-Yeh Lin

指導教授：儒森斯坦

Advisor : Prof. Baruch Rosenstein

國立交通大學

電子物理研究所



Submitted to Institute of Electrophysics

College of Science

National Chiao Tung University

For The Degree of Master of physics

in

Electrophysics

October 2007

Hsinchu, Taiwan, Republic of China

中華民國九十六年十月

Acknowledgments

在交大的這些日子裡，要感謝很多人給我幫忙和照顧。首先要謝謝我的指導教授 - 儒森斯坦教授，在我完全不懂這個領域的時候，是他一步一步指導我，教我算數學，還有給我很多模擬上的建議，並幫助我完成碩士學位，這兩年他很有耐心的為我解答問題並且給我很多重要的教導。還有北京大學的李定平教授，當我在北京大學的時候給我很多照顧及指導。實驗室的林佩真學姐陪我討論功課、研究上的瓶頸和計算問題。中原的學長和老師總是在我不知道要怎麼辦的時候給我建議和打氣。一直以來指導我寫程式的 KC，讓我的程式設計方面能克服困難以順利完成研究。特別要謝謝我的家人和朋友，爸媽、姐姐們，讓我有機會念書並完成學業，還有小喵喵陪伴我一起度過壓力最大的時候。最後要感謝高速電腦中心的福爾摩莎主機提供計算平台及帳號讓我能進行模擬及高速運算。

二維 Ginzburg-Landau 模型模擬第二類超導 的熱擾動和無序現象

研究生：林宏燁

指導教授：儒森斯坦 教授

國立交通大學

電子物理研究所



在本論文中，我們使用二維金斯堡-朗道模型及準動量基底來模擬二維第二類超導體，並由蒙地卡羅方法來分析研究其在熱擾動和無序影響下的行為。在有序條件下，我們計算了漩渦系統的 Abrikosov ratio、比熱、內能、漩渦的排列情況及結構係數。由於內能的分布圖呈現雙峰的結構，我們判斷系統的相變屬於弱一級相變，並且推論無限大系統的相變約化溫度 $t_m \sim -14.1$ 。藉由分析 Bragg peaks 在動量空間的行為，可以得知分別在液態和固態條件下漩渦的詳細排列狀況。我們測量了結構係數和溫度及系統尺寸的關係圖，分別得到了各系統的漩渦晶格熔點以及結構係數與溫度的代數關係。接著，對系統加入了一個隨機亂數場，使系統變成了無序的狀態。然後討論了有序和無序系統在漩渦排列和結構函數的差異處，並且更進一步的分析無序系統的磁化率來試著得到漩渦液態和玻璃態的分界線。

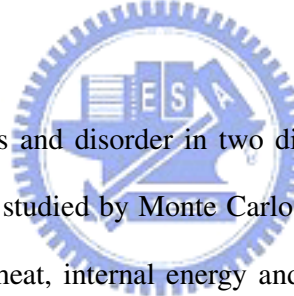
Thermal fluctuations and disorder in 2D Ginzburg-Landau model

Student : Hung-Yeh Lin

Adviser : Prof. Baruch Rosenstein

Institute of Electrophysics
National Chiao Tung University

Abstract



The thermal fluctuations and disorder in two dimensional Ginzburg-Landau model in the quasimomentum basis are studied by Monte Carlo simulation. In the pure vortex system, the Abrikosov ratio, specific heat, internal energy and structure factor were calculated. The melting phase transition is weakly first order as is inferred from a double - peak of the internal energy distribution. The melting reduced (dimensionless) temperature $t_m \sim -14.1$ is extrapolated for the infinite system size. The behavior of Bragg peaks indicates that the different of arrangement of solid and liquid states. The temperature and size dependence of structure factor shows the melting temperature t_m of flux-line-lattice and the algebraic relation of system size and structure factor. The δT_c disorder is simulated by adding the random potential field is added to the quadratic term of the GL energy. The difference between the pure and the disordered system is demonstrated by snapshots of the vortex configurations and the structure factor. I tried to locate the glass line of disorder system by analyzing the distribution of magnetization.

Contents

Acknowledgment	i
Abstract (Chinese version)	ii
Abstract (English version)	iii
Contents	iv
List of Figures	vi
List of Tables	vii
Chapter 1	Introduction	1
Chapter 2	Model and its major simplifications	6
2.1	Ginzburg - Landau free energy for constant magnetic field.....	6
2.2	Free energy expressed via variables in the quasimomentum basis. Clean case	9
2.3	Disorder term in the GL free energy.....	13
2.4	Thermal fluctuations	18
Chapter 3	Monte Carlo method	19
3.1	Metropolis algorithm.....	19
3.2	Monte Carlo simulation.....	20
Chapter 4	Results for the clean system subject to thermal fluctuations	21
4.1	Abrikosov ratio, hexagonal symmetry of the crystalline state.....	21

4.2	Normalized specific heat.....	23
4.3	Internal energy and its distribution.....	24
4.4	Vortices configuration and Structure factor.....	28
Chapter 5	Quenched disorder.....	35
5.1	Comparison of Structure factor with that of pure vortex system.....	35
5.2	The glass line of the disorder system.....	39
Chapter 6	Conclusion	43
Appendix	45
Appendix A	45
Appendix B	48
Appendix C	52
References	56



List of Figures

Figure 1-1.	Schematic magnetic phase diagram of a type II superconductor	2
Figure 2-1-1.	The general displacement vector of sqewed rectangle	8
Figure 2-3-1.	The distribution of the random potential in momentum space	15
Figure 4-1-1.	The relation between Abrikosov ratio β_A and reduce temperature a_T	22
Figure 4-2-1.	The normalized specific heat $\frac{C_v}{\Delta C_v}$ as a function of the reduce temperature a_T	23
Figure 4-3-1.	The dimensionless internal energy $\frac{\langle H \rangle}{T}$ versus reduce temperature a_T for vortex number $N_s = 256$	24
Figure 4-3-2.	The energy distribution $P(E)$ versus E with different vortex number.	26
Figure 4-3-3.	The history of normalized internal energy E with $N_s = 256, a_T = -13.02$	27
Figure 4-4-1.	The snapshots of $N_s = 256$ vortex position.	29
Figure 4-4-2.	The snapshots of the diffraction pattern $\langle \Delta(\mathbf{q}) ^2 \rangle$	31
Figure 4-4-3.	The structure factor $S(\mathbf{q})$ versus reduced temperature a_T for various system size.	32
Figure 4-4-4.	The structure factor $S(\mathbf{q})$ versus system size N_s for various reduced temperature a_T	33
Figure 4-4-5.	The dependence of melting temperature t_m on system size $N_s^{-1/2}$	34

Figure 5-1-1. The wave vector dependence of the structure factor for disordered system at $a_T = -15$35

Figure 5-1-2. The snapshots of the vortex position for various disorder systems.37

Figure 5-1-3. The structure factor $\overline{S(q)}$ in units $\frac{Tl^4}{2b'}$ versus reduce temperature a_T with $\tilde{\zeta} = 0.01$ for different system size.38

Figure 5-2-1. The phase diagram of vortex glass and vortex liquid which are separated by a_T^g curve.39

Figure 5-2-2. The system size dependence of magnetization for various a_T40

Figure 5-2-3. The system size dependence of second moments for various a_T41

Table 5-2-1 The Monte Carlo data of the nth moments and magnetization for various reduced temperature a_T42



List of Tables

Chapter 1 Introduction

Type II superconductors

Superconductivity is a phenomenon in which electrons pair together into Cooper pairs creating a coherent state with such remarkable properties as zero resistivity and perfect diamagnetism. According to the way a superconducting material responds to an external magnetic field, one can divided superconductors into two different classes: Type I and Type II. In type I superconductors below the critical value H_c magnetic flux is expelled from the bulk of the material (Meissner effect). Raising the external magnetic field past the critical value H_c , the Meissner effect is broken and the superconductivity is destroyed.

On the other hand in type II superconductor, there are three regions divided by two critical values $H_{c1}(T)$ and $H_{c2}(T)$ in magnetic phase diagram as shown in Fig. 1. When external magnetic field H is below H_{c1} , the Meissner effect exists in the superconductor, and the superconductive states have no resistance. In the region $H_{c1} < H < H_{c2}$ certain amount of the magnetic flux can penetrate the superconductor. The sample is divided into two states, normal areas (cores) and superconducting areas. At relatively small magnetic flux penetrates the material mostly in normal cores. The flux lines enter the material with vorticity quantized, the vortex was also called Abrikosov vortex or fluxion, each vortex carries one unit of flux $\Phi_0 = \frac{hc}{2e}$. This phenomenon is called mixed state or Shubnikov phase. The superconductivity is destroyed and there are no vortices in the superconductor while the strength of the external magnetic field H larger than the second critical value H_{c2} .

Because of type II superconductor can endure stronger magnetic than type I superconductor, the type II superconductor is quite practicable for both academic and industrial development.

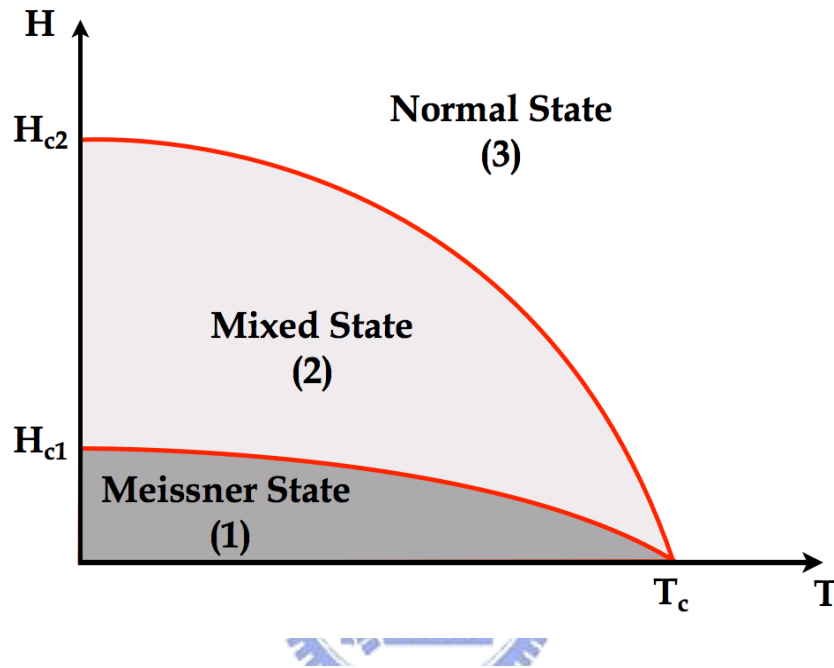


Fig. 1-1.
Schematic magnetic phase diagram of a type II superconductor.
(1) Meissner State (2) Mixed State (3) Normal State.


Abrikosov vortices in the mixed state, lattice and its melting

Two major characteristics of the mixed state are the coherence length ξ which is the size of the normal core and the London penetration depth λ on whose scale the supercurrent (current associated with Cooper pair) decays. The regular arrangement of the vortices is called Abrikosov lattice similar to an atomic lattice. Usually they arrange themselves in a form of hexagon to minimize mutual repulsion. If we raise the temperature above a certain value T_m , the Abrikosov lattice melts into the vortex liquid phase.

London and Ginsburg-Landau approximations

The two basic approximations to phenomenologically describe superconductivity on microscopic scale are London and Ginsburg-Landau approximations. The difference of these two approximations is that the London approximation assumes the constant order parameter and Ginsburg-Landau approximation uses the wave function to describe the order parameter with constant external magnetic field. Microscopic theories like the BCS theory for conventional s – wave superconductors, while can explain the phenomenon with homogeneous order parameter successfully, are too complicated to treat an inhomogeneous mixed state in external magnetic field, Ginsburg-Landau theory can describe the phenomenon of superconductor more easily.

Layered superconductors



Generally high T_c cuprites are layered materials, which consist of the copper-oxide planes. The electrons comprising Cooper pairs move mostly within the copper-oxide planes and the properties of superconductivities become largely two dimensional. The anisotropy parameter gamma is not very large in optimally doped YBCO ($\gamma = 5\sim 7$), but becomes very large for BSCCO or underdoped YBCO (of order 50 or higher). In this case, the thermal fluctuations are practically two dimensional. This is seen experimentally by the scaling of magnetization, specific heat etc. In addition many other layered materials (like organic superconductors) are also nearly two dimensional. Recently layered superconductor BSCCO became a major material for applications like the THz wave generator. In addition to its phenomenological significance, the 2D system is by far simpler to simulate compared to the 3D one (which is still rather inaccessible to the MC method).

Present work

This thesis focuses on the properties of the two dimensional type II superconductors with the external magnetic field in the region $H_{c1} \ll H < H_{c2}$. In this field range, the superposition of magnetic fields of vortices makes the internal field B nearly homogeneous. Moreover for $|H_{c2} - H| \ll H_{c2}$, the magnetic field is high enough so that so called higher Landau levels excitations can be neglected. Low energy states all belong to the lowest Landau level (LLL). Therefore we only consider the order parameter $\Psi(x, y)$ constrained to the LLL. In high T_c superconductors (and in some relatively low T_c layered materials), the thermal fluctuations on the microscopic scale are not negligible. Strongly thermal fluctuations on the microscopic scale affect such characteristics of the high temperature superconductors as specific heat, magnetization, structure factor etc. They lead to Abrikosov lattice melting and complicate the vortex matter phase diagrams. In real materials vortices are generally pinned by impurities creating disorder in the vortex system. Disorder determines the most important characteristic of a superconductor – critical current. The materials keep the main property of a superconductor, its zero resistance, only when the vortices are pinned. In this case the vortex system become a “vortex glass” or a ”Bragg glass”. Hence, it is important to find the glass line of the vortex system.

Previous simulation and theoretical results

The Monte Carlo simulations on phase transition of type II superconductor were done over the years by many researchers. Clean system in the presence of thermal fluctuations was simulated by Y. Kato and N. Nagaosa¹ who used the quasi-periodic boundary condition within the LLL approximation in Landau gauge. The finite size scaling of the algorithm was estimated to be N_s^{-2} (N_s is defined as the degrees of freedom). J .Hu and A. H. MacDonald⁹ used quasimomentum basis to speed up the simulation, so that the finite size scaling becomes N_s^{-1} . J .Hu and A. H. MacDonald, Kato and Nagaosa, found the first order phase transition from crystalline to liquid phase, by the double peak in probability of energy distribution $P(E)$.

Disordered system was first simulated only recently by M. S. Li and T. Nattermann³. They also claimed the model of the disorder system with expanding the random Gaussian disorder in Hermite polynomials. They presented the results of the flux lattice melting transition and the behavior of different correlation factor. They concluded that the phase transition from the curves of reduced temperature dependence of structure factor splayed out near the melting temperature. No glass transition was found for the highest value of disorder considered the disorder parameter $\tilde{\zeta} = 0.01$.

Theoretical estimates of melting temperature with and without disorder. D. Li, B. Rosenstein and V. Vinokur¹³ provided a theory to determine the glass transition in a disorder vortex system. In their theory, the behavior of the magnetization in vortex glass is different from the one in vortex liquid. I tried to find the glass line of a disorder system by analyzing this quantity.

There are six chapters in this thesis: the model of 2D the lowest Landau level GL free energy and quasi-momentum basis are introduced in Chapter 2. The Metropolis algorithm and the Monte Carlo calculations are shown in Chapter 3. The results and discussion of clean system are studied in Chapter 4. The vortex systems with disorder are analyzed in Chapter 5 and I discussed the conclusion in Chapter 6.

Chapter 2 Model and its major simplifications

2.1 Ginzburg Landau free energy for constant magnetic field

Our starting point is the two dimensional GL free energy:

$$F = \int dx dy \frac{\hbar^2}{2m} \left| \left(\nabla - \frac{ie^*}{\hbar c} \mathbf{A} \right) \Psi \right|^2 + \alpha'(T)(1 + U(x, y)) |\Psi|^2 + \frac{b'(T)}{2} |\Psi|^4 \quad (2.1.1)$$

here Ψ is the order parameter of the superconductivity, the gauge $A = (By, 0)$ describes a nonfluctuating constant magnetic field. m and e^* are the mass and charge of the Copper pair. $\alpha'(T) = \alpha T_c(1 - t)$ and $b'(T)$ are phenomenological parameters; $t \equiv T/T_c$.

Throughout most of the paper will use the following units. Unit of length is magnetic

length $l = \frac{\xi}{\sqrt{b}}$, the coherence length $\xi = \sqrt{\frac{\hbar^2}{2m\alpha T_c}}$ and unit of magnetic field is H_{c2} , so

that dimensionless magnetic field is $b \equiv \frac{B}{H_{c2}}$. I introduce weak so called δT_c disorder by

adding a space dependent contribution $U(x, y)$ to the coefficient of quadratic term.

Lowest Landau level approximation and quasimomentum basis

Expanding the field in quasimomentum basis only within the LLL¹²

$$\Psi(x, y) = \sum_k C_k \varphi_k, \quad (2.1.2)$$

$$\varphi_k = \sqrt{\frac{2\pi}{\sqrt{\pi}a}} \sum_{\kappa=-\infty}^{\infty} \exp \left\{ i \left[\frac{\pi\kappa(\kappa-1)}{2} + \frac{2\pi(x-k_y)}{a} \kappa - xk_x \right] - \frac{1}{2} \left(y + k_x - \frac{2\pi}{a} \kappa \right)^2 \right\}, \quad (2.1.3)$$

where the coefficients C_k are complex numbers and φ_k are quasi-momentum basis. We can find the property of φ_k easily

$$\varphi_k = \exp\{-ixk_x\} \varphi_0(x - k_y, y + k_x). \quad (2.1.4)$$

It is convention to prove that quasi-momentum basis satisfy magnetic translations¹⁸

which is defined as

$$T_{\mathbf{d}} \varphi_k = e^{i\mathbf{k} \cdot \mathbf{d}} \varphi_k, \quad (2.1.5)$$

here \mathbf{d} is a general displacement vector and $T_{\mathbf{d}}$ is magnetic translation operator.

$$T_{\mathbf{d}} = e^{-i\mathbf{d} \cdot \hat{\mathbf{P}}}, \quad (2.1.5)$$

with a generator defined by

$$\hat{P}_i = -i\partial_i - \mathcal{B}_{ji}r_j = \hat{p}_i - \mathcal{B}_{ji}r_j,$$

$$\mathcal{B} = \begin{bmatrix} 0 & b \\ 0 & 0 \end{bmatrix}, A_i = \mathcal{B}_{ij}r_j.$$

\mathcal{B} is the Landau gauge matrix.

The sample and periodic boundary conditions

My sample has following dimensions:

$$L = L\mathbf{d}_1 + L\mathbf{d}_2. \quad (2.1.6)$$

$$\mathbf{d}_1 = (a, 0), \quad \mathbf{d}_2 = a \left(\frac{1}{2}, \frac{\sqrt{3}}{2} \right). \quad (2.1.7)$$

here $a = \sqrt{\frac{4\pi}{\sqrt{3}}}$. Thus, the area of sqewed rectangle is $L^2 \mathbf{d}_1 \times \mathbf{d}_2 = 2\pi N_s$, $N_s = L^2$.

According to definition of \mathbf{d}_1 and \mathbf{d}_2 , the basis vectors $\tilde{\mathbf{d}}_1$ and $\tilde{\mathbf{d}}_2$ of the reciprocal lattice are

$$\tilde{\mathbf{d}}_1 = \frac{2\pi}{a} \left(1, -\frac{1}{\sqrt{3}} \right), \quad \tilde{\mathbf{d}}_2 = \frac{2\pi}{a} \left(0, \frac{2}{\sqrt{3}} \right). \quad (2.1.8)$$

we work in reciprocal lattice vector, so that \mathbf{k} with the basis vector is

$$\mathbf{k} = k_1 \tilde{\mathbf{d}}_1 + k_2 \tilde{\mathbf{d}}_2. \quad (2.1.9)$$

here $k_1 = 0, \frac{1}{L}, \dots, \frac{L-1}{L}$ and $k_2 = 0, \frac{1}{L}, \dots, \frac{L-1}{L}$ due to we choose the lowest Landau level wave function with quasi-momentum \mathbf{k} .

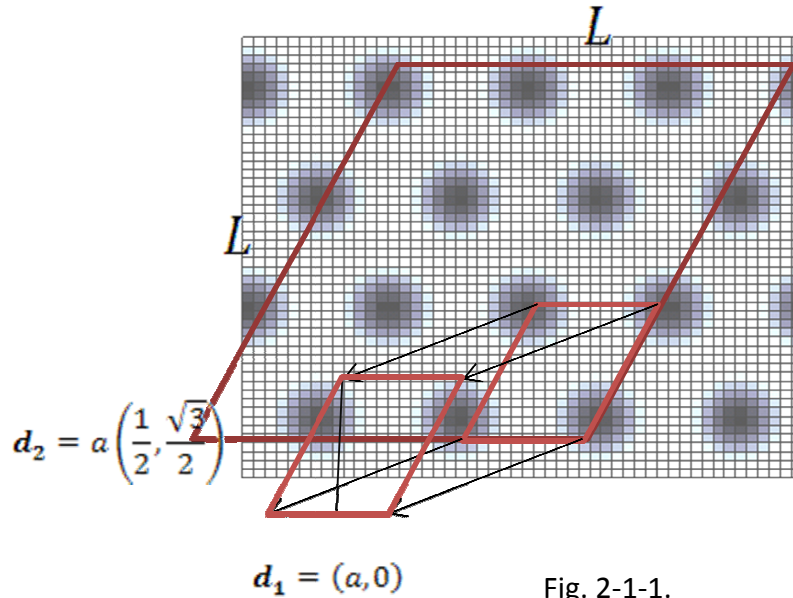


Fig. 2-1-1.

The general displacement vector of sqewed rectangle.

The quasi-momentum basis satisfy magnetic translations

$$T_L \Psi(x, y) = e^{ikL} \Psi(x, y) \quad (2.1.10)$$

and then we have

$$e^{ikL} = 1$$

$$k_x = \frac{2\pi}{L} n_x, n_x = 0, \pm 1, \pm 2, \dots$$

$$k_y = \frac{2\pi}{L} n_y, n_y = 0, \pm 1, \pm 2, \dots \quad (2.1.11)$$

Because of I used the LLL approximation, the ranges of n_x and n_y are

$$n_x = 0, 1, \dots, L - 1$$

$$n_y = 0, 1, \dots, L - 1$$

$$(2.1.12)$$

Thus, the basis satisfy magnetic translations and we have the periodic boundary condition.



2.2. Free energy expressed via quasimomentum variables. Clean case.

The GL free energy equation for pure vortex system is

$$F = \int dx dy \frac{\hbar^2}{2m} \left| \left(\nabla - \frac{ie^*}{\hbar c} A \right) \Psi \right|^2 + \alpha T_c (1 - t) |\Psi|^2 + \frac{b'}{2} |\Psi|^4. \quad (2.2.1)$$

In order to get the dimensionless LLL free energy, I rescaled $\Psi^2 \rightarrow \sqrt{\frac{T}{l^2 b' 4\pi}} \Psi^2$, $x \rightarrow \frac{x}{l}$,

$y \rightarrow \frac{y}{l}$, then we obtain

$$\frac{F}{T} = \frac{1}{4\pi} \int dx dy \left[a_T |\Psi|^2 + \frac{1}{2} |\Psi|^4 \right]. \quad (2.2.2)$$

here $a_T = \frac{2\alpha_\beta \pi^{1/2} l}{b^{1/2} T^{1/2}}$ is the reduced temperature, and $\alpha_\beta = \alpha T_c (1 - b - t)$.

I used some basic formulas¹⁸ to calculate the dimensionless GL free energy as follows.

The two function product is

$$\int_r dx \varphi(r) \varphi_k^*(r) \exp[-i\mathbf{r} \cdot \mathbf{q}] = 4\pi^2 \Delta_{\mathbf{q},\mathbf{k}} F(\mathbf{q}). \quad (2.2.3)$$

here

$$F(\mathbf{q}) = \exp\left[\frac{i\pi}{2}(Q_1^2 - Q_1)\right] \exp\left[-\frac{\mathbf{q}^2}{4b} - \frac{iq_x q_y}{2b} + \frac{ik_x q_y}{b}\right]. \quad (2.2.4)$$

and the Kronecker delta is defined by:

$$\Delta_{\mathbf{q},\mathbf{k}} = \Delta(\mathbf{q} - \mathbf{k}) = \begin{cases} 1, & \text{if } \mathbf{q} = \mathbf{k} + Q_1 \tilde{\mathbf{d}}_1 + Q_2 \tilde{\mathbf{d}}_2. \\ 0, & \text{otherwise} \end{cases}. \quad (2.2.5)$$

The momentum \mathbf{q} is composed of an “integer part”

$$\mathbf{Q} = Q_1 \tilde{\mathbf{d}}_1 + Q_2 \tilde{\mathbf{d}}_2. \quad (2.2.6)$$

$Q_1 = \dots, -1, 0, 1, \dots$, and $Q_2 = \dots, -1, 0, 1, \dots$, which belonging to the reciprocal lattice and a “fractional part”

$$\mathbf{k} = k_1 \tilde{\mathbf{d}}_1 + k_2 \tilde{\mathbf{d}}_2. \quad (2.2.7)$$

$k_1 = 0, \frac{1}{L}, \frac{2}{L}, \dots, \frac{L-1}{L}$ and $k_2 = 0, \frac{1}{L}, \frac{2}{L}, \dots, \frac{L-1}{L}$ which belongs to the Brillouin zone.

The inverse Fourier transform of Eq.(2.2.3) is

$$\begin{aligned} \varphi_0(r) \varphi_k^*(r) = & \sum_{Q_1 \tilde{\mathbf{d}}_1 + Q_2 \tilde{\mathbf{d}}_2} \exp[i(\mathbf{k} + \mathbf{Q}) \cdot \mathbf{r}] \exp\left[\frac{\pi i}{2}(Q_1^2 + Q_1)\right] \exp\left[-\frac{(\mathbf{k} + \mathbf{Q})^2}{4}\right. \\ & \left. - \frac{i(k_x + Q_x)(k_y + Q_y)}{2} + ik_x(k_y + Q_y)\right]. \end{aligned} \quad (2.2.8)$$

The quadratic term of GL free energy is

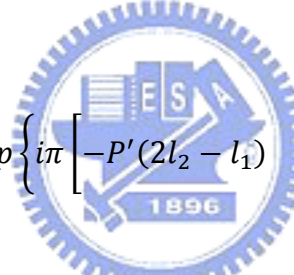
$$\rho(x, y) = |\psi(x, y)|^2 = \sum_{\mathbf{k}, \mathbf{l}} C_{\mathbf{k}} C_{\mathbf{l}} \varphi_{\mathbf{k}} \varphi_{\mathbf{l}}. \quad (2.2.9)$$

It can be verified by using Eq.(2.1.4) and Eq.(2.2.8) to Eq.(2.2.9), see Appendix A, that

$$\begin{aligned} \rho(x, y) = & \sum_{\mathbf{k}, \mathbf{l}} \sum_{\mathbf{Q}} \exp\{il_y(k_x - l_x)\} \exp[i(k_x - l_x + Q_x)x + i(k_y - l_y + Q_y)y \\ & - i(k_x - l_x + Q_x)l_y] \exp\left[\frac{i\pi}{2}(Q_1^2 - Q_1)\right] \exp\left[-\frac{(\mathbf{k} - \mathbf{l} + \mathbf{Q})^2}{4}\right. \\ & \left. - \frac{i(k_x - l_x + Q_x)(k_y - l_y + Q_y)}{2} + ik_x(k_y - l_y + Q_y)\right] C_{\mathbf{k}}^* C_{\mathbf{l}}. \end{aligned} \quad (2.2.10)$$

and then calculated $\tilde{\rho}(\mathbf{p} + \mathbf{P})$ as the fourier transform of $\rho(x, y)$, see Appendix B, we

have



$$\begin{aligned} \tilde{\rho}(\mathbf{p} + \mathbf{P}) = & \sum_{\mathbf{l}} \exp\left\{i\pi \left[-P'(2l_2 - l_1) \right. \right. \\ & \left. \left. + \frac{1}{2}(p_1 + 2l_1 - P'')[2(p_2 + P_2) - (p_1 + P_1)] \right] \right\} \exp\left[\frac{i\pi}{2}(P'^2 \right. \\ & \left. - P')\right] \exp\left[-\frac{(\mathbf{p} + \mathbf{P})^2}{4}\right] C_{[p_1+l_1], [p_2+l_2]}^* C_{\mathbf{l}}. \end{aligned} \quad (2.2.11)$$

with two conditions :

1. if $(p_1 + l_1) < 1 \rightarrow P' = P_1, P'' = P_1,$
2. if $(p_1 + l_1) > 1 \rightarrow P' = P_1 + 1, P'' = P_1 + 2.$

Thus, the inverse Fourier transform of $\tilde{\rho}(x, y)$ is

$$\rho(x, y) = \sum_{\mathbf{p} + \mathbf{P}} \tilde{\rho}(\mathbf{p} + \mathbf{P}) \exp[i(\mathbf{p} + \mathbf{P}) \cdot \mathbf{r}]. \quad (2.2.12)$$

We turn back to calculate the terms of GL free energy.

Quadratic term

$$\begin{aligned} \frac{1}{4\pi} \int_{x,y} a_T |\Psi(x,y)|^2 &= \frac{a_T}{4\pi} \int_{x,y} \sum_{\mathbf{p}+\mathbf{P}} \tilde{\rho}(\mathbf{p}+\mathbf{P}) \exp[i(\mathbf{p}+\mathbf{P}) \cdot \mathbf{r}] = \frac{a_T}{4\pi} [2\pi L^2 \tilde{\rho}(\mathbf{0})] \\ &= \frac{a_T}{2} L^2 \sum_l C_l^* C_l. \end{aligned}$$

(2.2.13)

Quartic term

$$\begin{aligned} \frac{1}{8\pi} \int_{x,y} |\Psi(x,y)|^4 &= \frac{1}{8\pi} \int_{x,y} \sum_{\mathbf{p}+\mathbf{P}} \tilde{\rho}(\mathbf{p}+\mathbf{P}) \exp[i(\mathbf{p}+\mathbf{P}) \\ &\cdot \mathbf{r}] \sum_{\mathbf{p}'+\mathbf{P}'} \tilde{\rho}(\mathbf{p}'+\mathbf{P}') \exp[i(\mathbf{p}'+\mathbf{P}') \cdot \mathbf{r}] = \frac{1}{4} L^2 \sum_{\mathbf{p}+\mathbf{P}} \tilde{\rho}(\mathbf{p}+\mathbf{P}) \tilde{\rho}^*(\mathbf{p}+\mathbf{P}) \\ &= \frac{1}{4} L^2 \sum_{\mathbf{p}+\mathbf{P}} |\tilde{\rho}(\mathbf{p}+\mathbf{P})|^2. \end{aligned}$$

(2.2.14)

Substitute (2.2.11) into (2.2.14), we have

$$\begin{aligned}
& \frac{1}{8\pi} \int_{x,y} |\Psi(x,y)|^4 \\
&= \frac{1}{4} L^2 \sum_{\mathbf{p}, \mathbf{P}} \left| \sum_l \exp \left\{ i\pi \left[-P'(2l_2 - l_1) \right. \right. \right. \\
&\quad \left. \left. \left. + \frac{1}{2}(p_1 + 2l_1 - P'')[2(p_2 + P_2) - (p_1 + P_1)] \right] \right\} \exp \left[\frac{i\pi}{2} (P'^2 \right. \right. \\
&\quad \left. \left. - P') \right] \exp \left[-\frac{(\mathbf{p} + \mathbf{P})^2}{4} \right] C_{[p_1+l_1],[p_2+l_2]}^* C_l \right|^2.
\end{aligned} \tag{2.2.15}$$

The detail calculation of dimensionless Ginzburg Landau free energy for pure vortex system is shown by previous work. Next, we calculate the disorder term and define the dimensionless parameter $\tilde{\zeta}$ which controls the relative disorder strength.



2.3 Disorder term in the GL free energy

The disorder term of GL free energy function is

$$\int_{x,y} \alpha T_c (1-t) U(x,y) |\Psi|^2. \tag{2.3.1}$$

with white noise correlator.

$$\overline{U(x,y)U(0,0)} = R\delta(x)\delta(y). \tag{2.3.2}$$

Rescaling field as $\Psi^2 \rightarrow \sqrt{\frac{T}{l^2 b' 4\pi}} \Psi^2$ and setting dimensionless lengths via $x \rightarrow \frac{x}{l}$, $y \rightarrow \frac{y}{l}$,

we obtain the disorder term of dimensionless GL free energy equation:

$$\int_{x,y} W(x,y) |\Psi|^2. \tag{2.3.3}$$

Here

$$W(x, y) = \frac{l\alpha T_c(1-t)}{2(\pi b'T)^{1/2}} U(x, y). \quad (2.3.4)$$

According to Eq. (2.3.3), we have the following variance

$$\overline{W(x, y)W(0,0)} = R'\delta(x)\delta(y), \quad (2.3.5)$$

where $R' = \left[\frac{l\alpha T_c(1-t)}{2(\pi b'T)^{1/2}} \right]^2 R$.

Representation of the random potential in terms of a complex random numbers

I used the random potential in the disorder term of GL equation as

$$\begin{aligned}
 U(x, y) = & a_{0,0,0,0} \\
 & + \sum_{p_1>0, P_1\geq 0, p_2=0, P_2=0} \{ a_{p_1,0,P_1,0} \exp[i(\mathbf{p} + \mathbf{P}) \cdot \mathbf{r}] \\
 & + a_{p_1,0,P_1,0}^* \exp[-i(\mathbf{p} + \mathbf{P}) \cdot \mathbf{r}] \} \\
 & + \sum_{p_2+P_2>0} \{ a_{\mathbf{p},\mathbf{P}} \exp[i(\mathbf{p} + \mathbf{P}) \cdot \mathbf{r}] + a_{\mathbf{p},\mathbf{P}}^* \exp[-i(\mathbf{p} + \mathbf{P}) \cdot \mathbf{r}] \}.
 \end{aligned} \quad (2.3.6)$$

here a is the complex random numbers, $a_{\mathbf{p}+\mathbf{P}} = a_{-(\mathbf{p}+\mathbf{P})}^*$

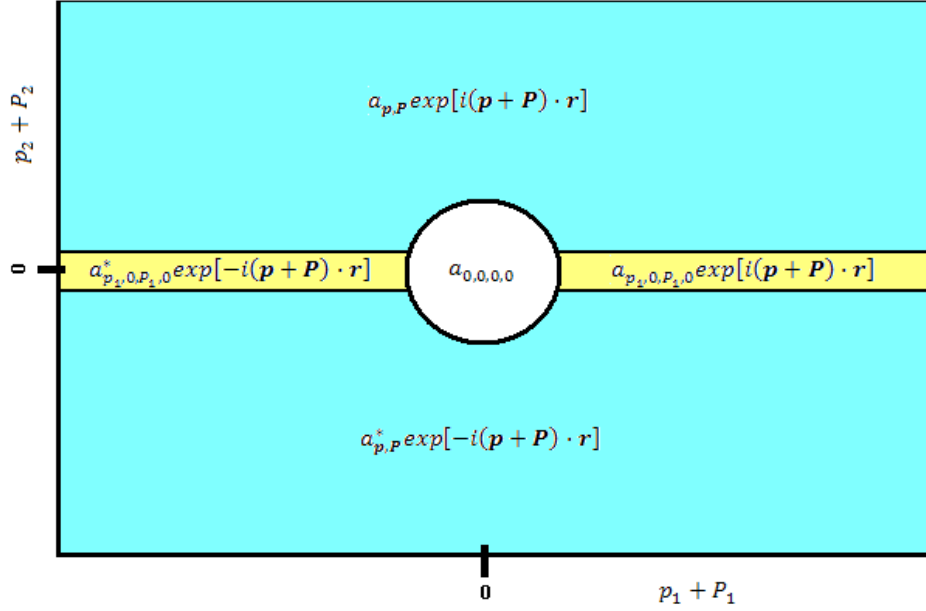


Fig. 2-3-1.
The distribution of the random potential in momentum space

and its distribution is divided into five parts, see Fig. 2-3-1. The white noise correlator is

$$\begin{aligned}
 \overline{U(x,y)U(0,0)} &= \overline{a_{0,0,0,0}^2} \\
 &+ \sum_{p_1 > 0, P_1 \geq 0, p_2 = 0, P_2 = 0} \{ a_{p_1,0,P_1,0}^* a_{p_1,0,P_1,0} \exp[i(\mathbf{p} + \mathbf{P}) \cdot \mathbf{r}] \\
 &+ a_{p_1,0,P_1,0} a_{p_1,0,P_1,0}^* \exp[-i(\mathbf{p} + \mathbf{P}) \cdot \mathbf{r}] \} \\
 &+ \sum_{p_2 + P_2 > 0} \{ a_{p,P}^* a_{p,P} \exp[i(\mathbf{p} + \mathbf{P}) \cdot \mathbf{r}] + a_{p,P} a_{p,P}^* \exp[-i(\mathbf{p} + \mathbf{P}) \cdot \mathbf{r}] \}.
 \end{aligned} \tag{2.3.7}$$

with some basic relations as follows:

$$\begin{aligned}
 \overline{a_{0,0,0,0}^2} &= \frac{R}{2\pi L^2}, \\
 \overline{Rea^2} = \overline{Ima^2} &= \frac{1}{2} \frac{R}{2\pi L^2} = \sigma^2,
 \end{aligned} \tag{2.3.8}$$

here σ^2 is the variance of the normal distribution. Substituting Eq.(2.2.11), Eq.(2.3.4) and Eq.(2.3.6) into Eq.(2.3.2), the disorder term of dimensionless GL free energy equation is

$$\begin{aligned}
& \int_{x,y} W(x,y)|\Psi(x,y)|^2 \\
&= 2\pi L^2 \frac{l\alpha T_c(1-t)}{2(\pi b'T)^{1/2}} \left\{ \tilde{\rho}(0)a_{0,0,0,0} \right. \\
&+ \sum_{p_1>0, P_1\geq 0, p_2=0, P_2=0} \{ \tilde{\rho}(\mathbf{p} + \mathbf{P})a_{p_1,0,p_1,0}^* + c. c. \} \\
&+ \left. \sum_{p_2+P_2>0} \{ \tilde{\rho}(\mathbf{p} + \mathbf{P})a_{p,P}^* + c. c. \} \right\}.
\end{aligned} \tag{2.3.9}$$

Relation to the disorder parameter $\tilde{\zeta}$ of Li and Nattermann

M. S. Li and T. Nattermann³ defined the dimensionless parameter $\tilde{\zeta}$ to control the relative disorder strength, and expand the random Gaussian disorder in renormalized Hermite polynomials to express the disorder term of GL free energy equation. In order to use the disorder parameter $\tilde{\zeta}$ in our simulation, I calculated the relation equation of standard deviation σ and disorder parameter $\tilde{\zeta}$. The disorder term of M. S. Li and T. Nattermann is

$$\int d^2r \alpha \delta T_c(r) |\Psi|^2, \tag{2.3.10}$$

here $\delta T_c(r)$ is real and Gaussian distributed with

$$\overline{\delta T_c(r)} = 0,$$

$$\overline{\delta T_c(r)\delta T_c(r')} = \zeta^2 T_c^2 \xi^2 \delta_\xi(r - r'). \quad (2.3.11)$$

The typical fluctuations $\delta T_c(r) \cong \zeta T_c$ of the mean field transition temperature. They defined the disorder parameter with following relation

$$\tilde{\zeta} = \zeta \frac{b^{1/2}}{\pi^{1/2}(1-t-b)}. \quad (2.3.12)$$

Connecting our disorder term with their notation, we have

$$R' = \frac{l^2 \alpha^2}{4\pi b' T} \zeta^2 T_c^2 \xi^2, \quad (2.3.13)$$

use the reduce temperature a_T we can rewrite R as follows

$$R' = \frac{l^2}{16\pi} a_T^2 \tilde{\zeta}^2, \quad (2.3.14)$$

and substitute Eq.(2.3.14) into Eq.(2.3.8)

$$\left[\frac{l\alpha T_c(1-t)}{2(\pi b' T)^{1/2}} \right]^2 \sigma^2 = \frac{l^2}{64\pi^2 L^2} a_T^2 \tilde{\zeta}^2. \quad (2.3.15)$$

Thus, we have the relation between standard deviation σ and disorder parameter $\tilde{\zeta}$. By controlling the specific $\tilde{\zeta}$ to generate the corresponding complex random fields, we can get various degree disorder vortex systems.

2.4 Thermal fluctuations

The general form for partition is

$$Z = \sum_{all\ states} e^{-\mathcal{H}/k_B T}, \quad (2.4.1)$$

where \mathcal{H} is the Hamiltonian for the system, T is the temperature, and k_B is the Boltzmann constant. The partition function is

$$\begin{aligned} Z &= \int \mathcal{D}\psi^*(x, y) \mathcal{D}\psi(x, y) \exp\left(\frac{-\mathcal{H}}{k_B T}\right) \\ &= \int \left(\prod_l dReC_l dImC_l \right) \exp \left[- \left\{ \frac{a_T}{2} L^2 \sum_l C_l^* C_l \right. \right. \\ &\quad + \frac{1}{4} L^2 \sum_{\mathbf{p}, \mathbf{P}} \left[\sum_l \exp \left\{ i\pi \left[-P'(2l_2 - l_1) \right. \right. \right. \\ &\quad \left. \left. \left. + \frac{1}{2} (p_1 + 2l_1 - P'') [2(p_2 + P_2) - (p_1 + P_1)] \right] \right\} \exp \left[\frac{i\pi}{2} (P'^2 \right. \right. \right. \\ &\quad \left. \left. \left. - P') \right] \exp \left[- \frac{(\mathbf{p} + \mathbf{P})^2}{4} \right] C_{[p_1+l_1], [p_2+l_2]}^* C_l \right|^2 \right] \right]. \end{aligned} \quad (2.4.2)$$

We can use Eq.(2.4.2) to calculate the thermodynamic quantities. For example, the average of energy is

$$\langle \mathcal{H} \rangle = \frac{\sum_{all\ states} \mathcal{H} e^{-\frac{\mathcal{H}}{k_B T}}}{Z}. \quad (2.4.3)$$

Chapter 3 Monte Carlo Method

3.1 Metropolis algorithm

The standard Monte Carlo method with Metropolis algorithm²¹ was used to simulate the two-dimensional pure and disordered vortex system. In the classic Metropolis method, we use a transition probability which depends on the difference of energy ΔE between the initial and trial configuration to determine whether the trial configuration is accepted or not. Now I introduce my Monte Carlo method as follows. First, we choose an initial configuration and calculate the initial energy E_m . Second, we choose a site $C_j \in \mathcal{C}^{N_s}$ randomly and generate the trial configuration with C_j^{new} by using the rule: $C_j^{new} \rightarrow C_j^{old} + \epsilon \Delta C$, where ΔC is a complex number which is chosen randomly from the region $|Re\Delta C| \leq 1$ and $|Im\Delta C| \leq 1$ in the complex plane. Third, we calculate the energy E_n of trial configuration and the difference of energy ΔE , here $\Delta E = E_n - E_m$. If $\Delta E \leq 0$, the system accepted the trial configuration, but if $\Delta E > 0$, the trial configuration is accepted with a probability $\exp(-\beta\Delta E)$. Generating a random number r uniformly in the interval $[0, 1]$, if $r \leq \exp(-\beta\Delta E)$ the trial configuration is accepted, otherwise it is rejected. This process is called Monte Carlo step/site (MCS/site). Note that the old configuration is still counted again for averaging if the trial configuration is rejected. By using Monte Carlo method, the system will fall into the stable states and reach the equilibration, and the characteristics of vortex system can be measured.

3.2 Monte Carlo calculations

I used Eq.(3.2.1) to vary the value of a specific wave function coefficient C_j in our Monte Carlo simulation

$$C_{l_1, l_2}^{new} = C_{l_1, l_2}^{old} + \delta_{l_1 - j_1} \delta_{l_2 - j_2} \Delta, \quad (3.2.1)$$

here $\Delta = \epsilon \Delta C$. Note that \mathbf{j} and \mathbf{l} are vectors which composed of two reciprocal vectors \tilde{d}_1 and \tilde{d}_2 . Furthermore we used Eq.(3.2.1) to calculate the energy of trial configuration and only discussed the changes of the summation of wave function coefficient product, the detail of Monte Carlo calculations are worked out in Appendix C. The summation of wave function coefficient product of trial configuration is

$$\begin{aligned} \sum_{l_1, l_2} C_{l_1, l_2}^{new*} C_{l_1, l_2}^{new} &= \sum_{l_1, l_2} (C_{l_1, l_2}^{old} + \delta_{l_1 - j_1} \delta_{l_2 - j_2} \Delta)^* (C_{l_1, l_2}^{old} + \delta_{l_1 - j_1} \delta_{l_2 - j_2} \Delta) \\ &= \sum_{l_1, l_2} (C_{l_1, l_2}^{old} C_{l_1, l_2}^{old*} + \delta_{l_1 - j_1} \delta_{l_2 - j_2} C_{l_1, l_2}^{old*} \Delta + \delta_{l_1 - j_1} \delta_{l_2 - j_2} C_{l_1, l_2}^{old} \Delta^* + \Delta \Delta^*) \\ &= C_{j_1, j_2}^{old*} \Delta + C_{j_1, j_2}^{old} \Delta^* + \Delta \Delta^* + \sum_{l_1, l_2} C_{l_1, l_2}^{old} C_{l_1, l_2}^{old*}. \end{aligned} \quad (3.2.2)$$

Evidently $\sum_{l_1, l_2} C_{l_1, l_2}^{old} C_{l_1, l_2}^{old*}$ term of Eq.(3.2.2) can be calculated directly by old configuration, hence we can store it to simulate the vortex system more efficiently. The old calculation results always can be applied in new one and a lot of computer time is saved, the CPU time in one Monte Carlo step $\propto L^2$. There are six different size ($4 \times 4, 6 \times 6, 8 \times 8, 10 \times 10, 12 \times 12, 16 \times 16$ numbers of vortices) systems in our simulation. We took $5 \times 10^5 \sim 1 \times 10^6$ MC steps to reach the thermal equilibration and calculated the physical quantities over $1 \times 10^6 \sim 1 \times 10^7$ MC steps. The physical quantities were measured every

30 ~ 50 MC steps. We control ϵ in a reasonable region to make the acceptance ratio is 0.3 ~ 0.4 and then the vortex system reach the thermal equilibrium state efficiently. All the simulations were started from the heating processes with the initial configuration which is defined as follows: $C_i = \sqrt{\frac{|a_T|}{\bar{\beta}_A}}$, here C_i is one of all coefficients of wave function and others are equal to zero, $\bar{\beta}_A \sim 1.16$ is the mean-field value of the Abrikosove ratio.

Chapter 4 Results for the clean system subject to thermal fluctuations

4.1 Abrikosov ratio, hexagonal symmetry

Abrikosov ratio explains the configuration of the vortex system. At low temperature, the system is in solid state and the vortices are arrayed regular as a atomic lattice, otherwise the vortices are arrayed as liquid in high temperature region. The definition of Abrikosov ratio is

$$\beta_A = \frac{1}{V} \frac{\langle \int_x |\psi(x)|^4 \rangle}{\left[\langle \int_x |\psi(x)|^2 \rangle \right]^2}. \quad (4.1.1)$$

The results of Abrikosov ratio for different size are shown in Fig. 4-1-1. The value of β_A is close to the mean-field value 1.16 at low temperature and the vortices are close to each other. It explains that my Monte Carlo simulation is reasonable. The Monte Carlo data of various size system N_s are collapse onto a single curve unless a_T near the melting

temperature. Note that the curves of the larger system size have slightly jumps while $a_T \sim t_m$.

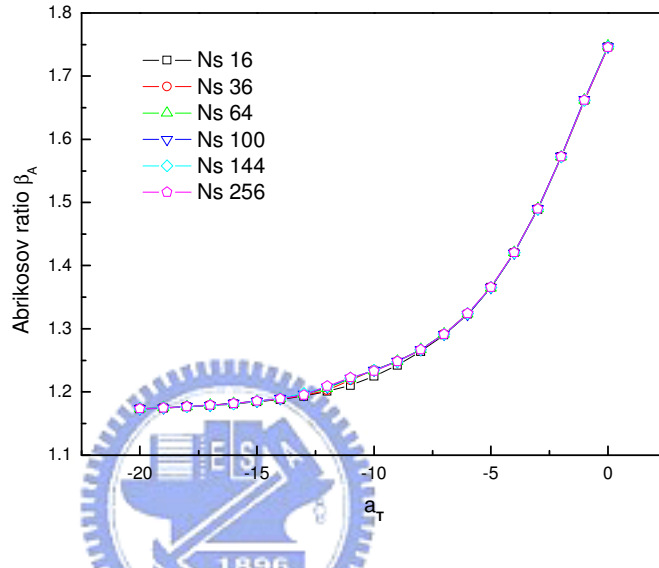


Fig. 4-1-1.

The relation between Abrikosov ratio β_A and reduce temperature a_T . The squares, circles, triangles, inverted triangles, diamonds and pentangle correspond to system size $N_s = 16, 36, 64, 100, 144, 256$. All data are in the same curve unless $a_T \sim t_m$, this phenomenon indicates the size dependence is negligible.

4.2 Normalized specific heat

The definition of normalized specific heat is $\frac{C_v}{\Delta C_v}$. Here

$$C_v = \frac{1}{V} \left[\left\langle \left[\frac{\partial H}{\partial T} \right]^2 \right\rangle - \left\langle \frac{\partial H}{\partial T} \right\rangle^2 \right], \quad (4.2.1)$$

which is the specific heat from the energy fluctuation and ΔC_v is the mean-field value of the specific heat. The results of normalized specific heat for different size are shown in Fig. 4-2-1. The curve has a pick indicates that the vortex systems have a melting transition near the melting temperature. In high temperature region (above t_m), the normalized specific heat decays quickly.

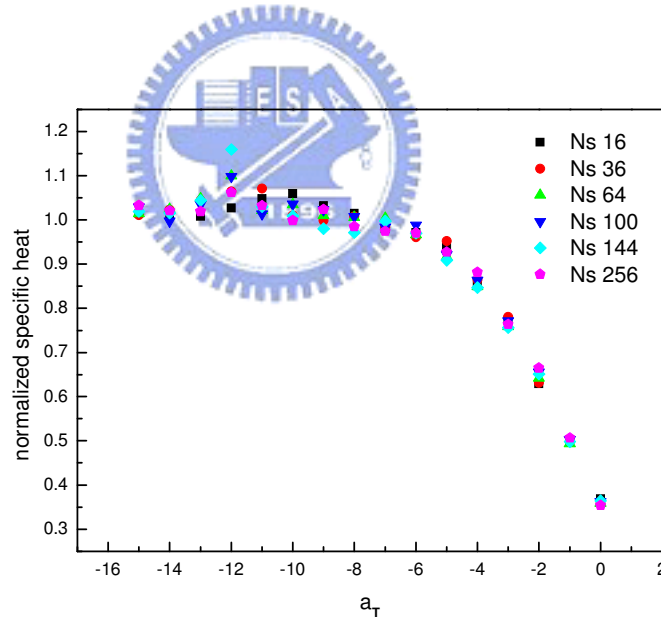


Fig. 4-2-1.

The normalized specific heat $\frac{C_v}{\Delta C_v}$ as a function of the reduce temperature a_T . The squares, circles, triangles, inverted triangles, diamonds and pentangle correspond to system size $N_s = 16, 36, 64, 100, 144, 256$.

4.3 Internal energy and its distribution

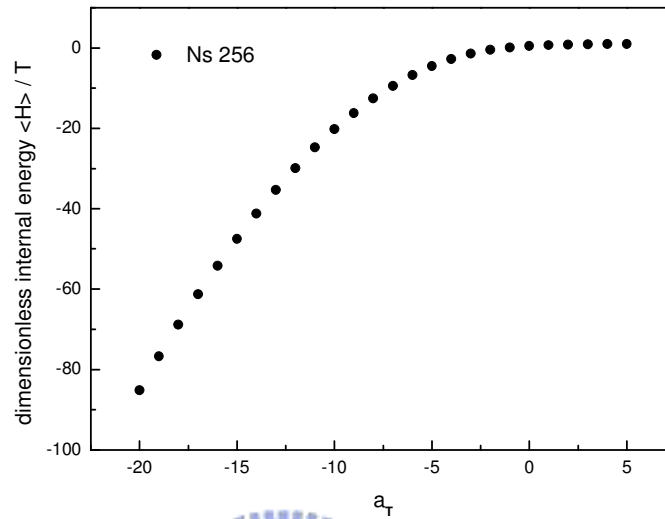


Fig. 4-3-1.

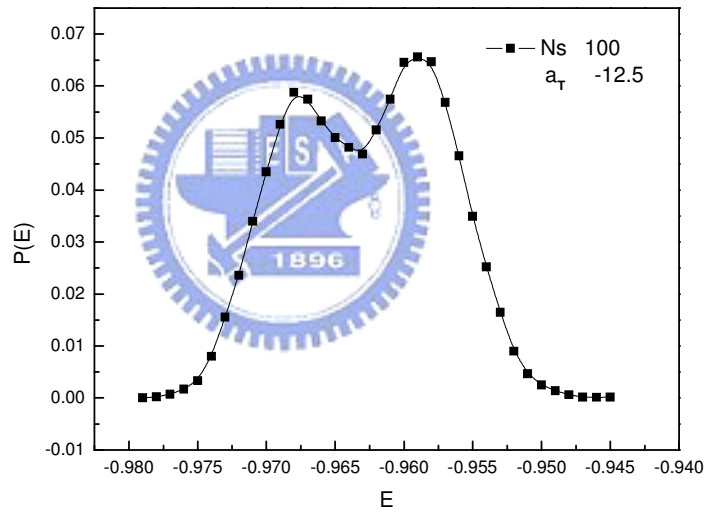
The dimensionless internal energy $\frac{\langle H \rangle}{T}$ versus reduce temperature a_T for vortex number $N_s = 256$.

Internal energy for $N_s = 256$ vortex system

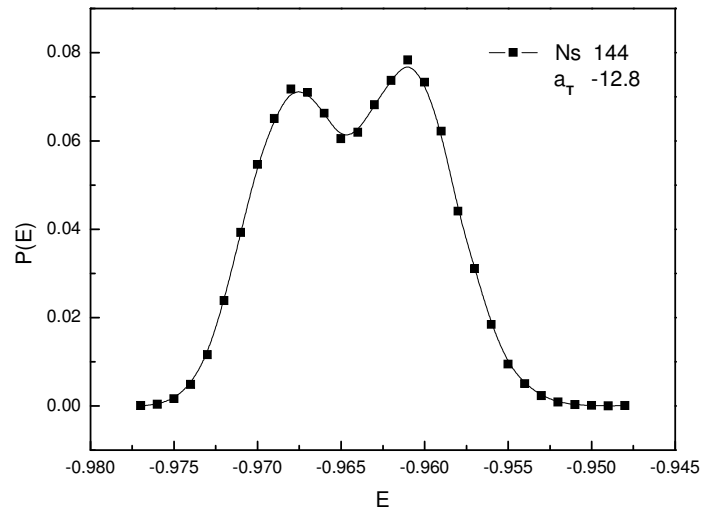
The results of the dimensionless internal energy for $N_s = 256$ are shown in Fig. 4-3-1. I took 3×10^6 Monte Carlo steps to measure this quantity, and used 3×10^6 Monte Carlo steps for the equilibration. My Monte Carlo data are very close to the results which were obtained by Kato and Nagaosa and then the simulation method which I used is reasonable. Note that I didn't find the indication of phase transition in the results. In order to discuss the phase transition of 2D vortex system, I measured the probability of energy distribution $P(E)$ and the history of normalized internal energy.

The probability of energy distribution $P(E)$

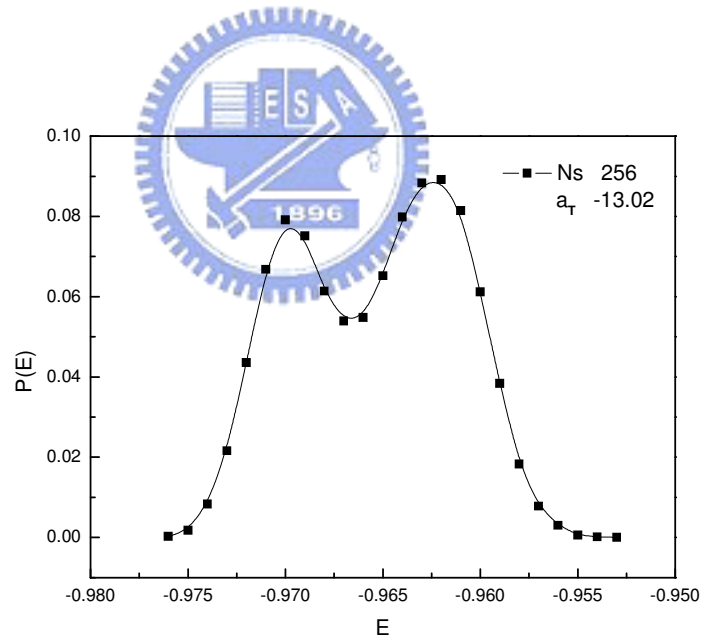
The probability of energy distribution $P(E)$ for various system sizes are shown in Fig. 4-3-2. As the result, $P(E)$ has a double-peak, the right peak corresponds to higher energy which represents the liquid phase and left peak corresponds to lower energy which represents the solid phase. The double-peak distribution indicates that the vortex system has a first order phase transition when $a_T \sim t_m$ (here $a_T = -12.5$ for $N_s = 100$, $a_T = -12.8$ for $N_s = 144$, $a_T = -13.02$ for $N_s = 256$).



(a)



(b)



(c)

Fig. 4-3-2.

The energy distribution $P(E)$ versus E with different vortex number: (a) $N_s = 100$, (b) $N_s = 144$, (c) $N_s = 256$. Each temperature approach the melting temperature of different N_s and the double peak is suggests that the first order phase transition exists in the melting process of the vortex lattice.

The history of the internal energy

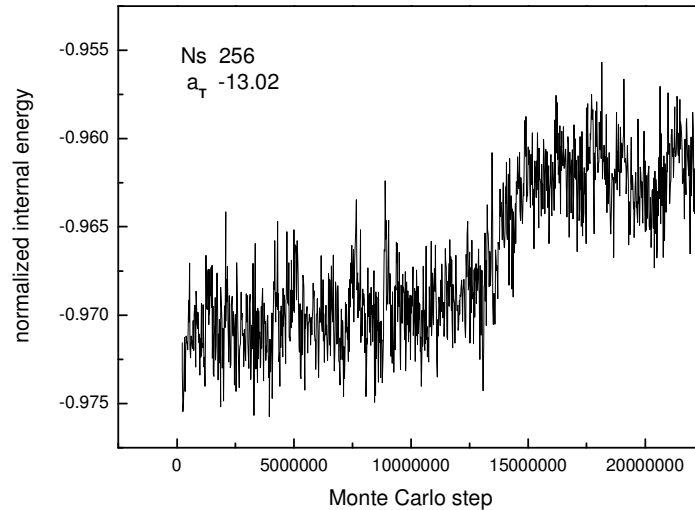


Fig. 4-3-3.

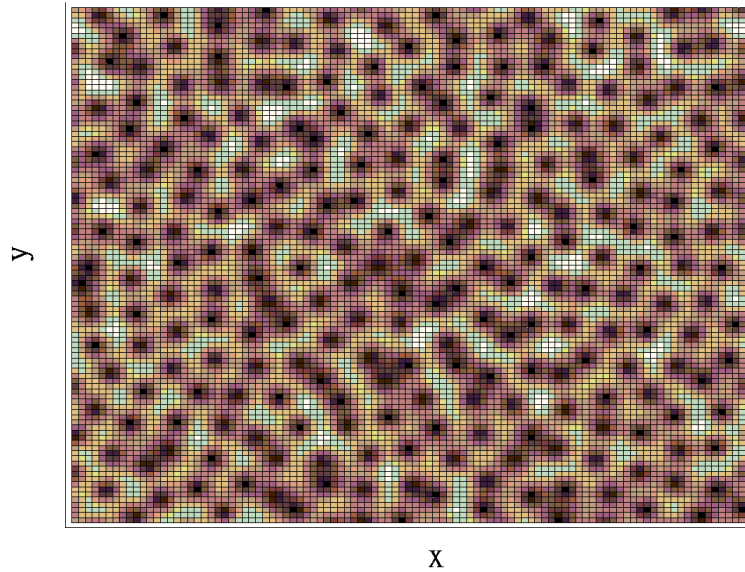
The history of normalized internal energy E with $N_s = 256$, $a_T = -13.02$. The sharp transition exists between the two regions with different energy. This phenomenon suggests the first order phase transition exists in the melting process.

Fig. 4-3-3 shows the history of the normalized internal energy of $N_s = 256$ vortex system at $a_T = -13.02$, we applied the solid initial condition to simulate the vortices system and recorded the internal energy every Monte Carlo step. Note that we used 2×10^5 Monte Carlo steps to reach the equilibrium which are not shown in the result. The relaxation processes consists two regions and a sharp transition region. The lower internal energy region corresponds to the metastable state while the higher internal energy corresponds to the stable one. Because of the sharp transition region is between the other two regions, the first order phase transition actually exists in the two locally stable states.

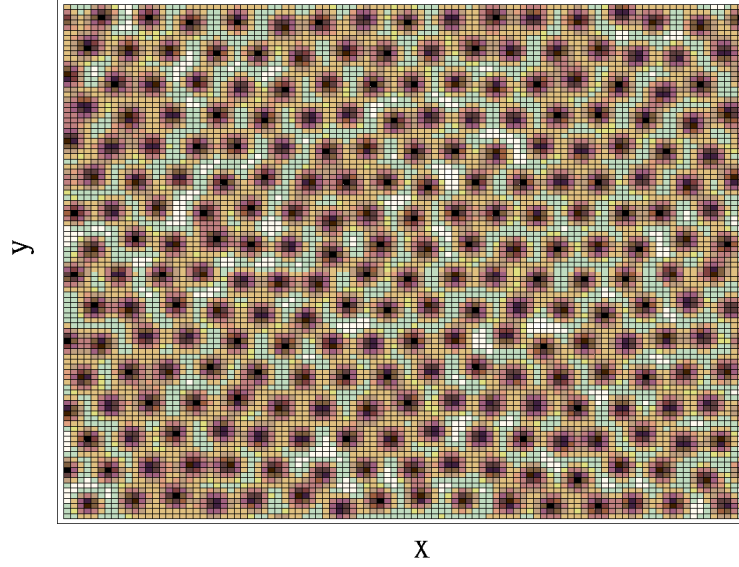
4. 4 Vortices configuration and Structure factor

Vortices configuration

In Fig. 4-4-1, we shown the snapshots of the spatial distribution of the magnitude of the order-parameter field $|\psi(x, y)|^2$ for $a_T > t_m$ and $a_T < t_m$. There are 256 vortices in each system and we used 1×10^6 Monte Carlo steps to reach the equilibration. I plotted the snapshots in the form of a rectangle. The range of x and y is $0 \sim L_x$ and $0 \sim L_y$, respectively, here $L_x = 3^{1/4} \pi^{1/2} L$ and $L_y = 2\pi^{1/2} L / 3^{1/4}$. As the results, (a) the vortices are arrayed regular like a lattice at $a_T = -15 < t_m$, otherwise (b) they arrayed randomly at $a_T = -8 > t_m$.



(a)



(b)

Fig. 4-4-1

The snapshots of $N_s = 256$ vortex position for (a) liquid state at $a_T = -8$ (b) solid state at $a_T = -15$. The range of X and Y is $0 \sim L_x$ and $0 \sim L_y$ respectively and the dark spots correspond to vortex cores.



We transfer the spatial distribution into the momentum space by Fourier transform.

The Fourier transform of the density-density correlation function is shown as follows

$$\chi_{DD}(\mathbf{q}) = \int_r \int_{r'} \langle |\psi(r)|^2 |\psi(r')|^2 \rangle e^{-i\mathbf{q}(r-r')}. \quad (4.4.1)$$

We transformed Eq.(4.4.1) into the other form

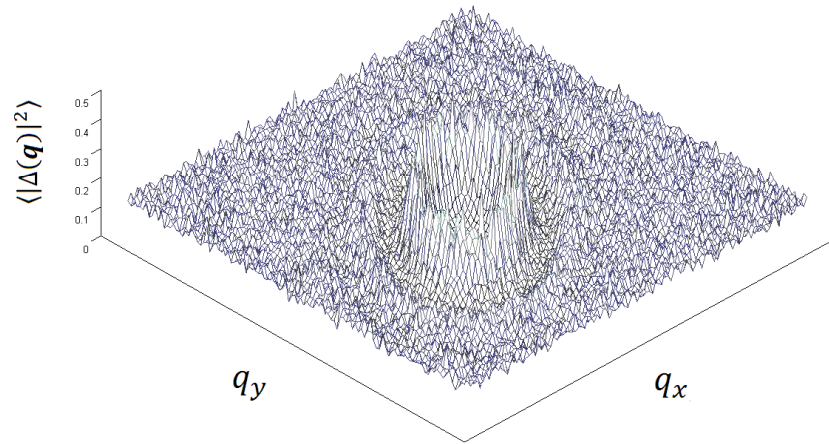
$$\chi_{DD}(\mathbf{q}) = 4\pi^2 L^4 e^{-\mathbf{q}^2/2} \langle |\Delta(\mathbf{q})|^2 \rangle, \quad (4.4.2)$$

with

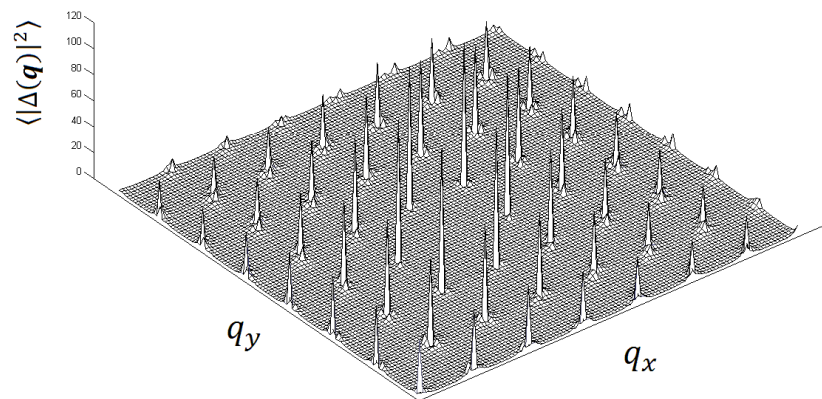
$$\begin{aligned}
\Delta(\mathbf{q}) = \sum_{\mathbf{l}} \exp \left\{ i\pi \left[-P'(2l_2 - l_1) \right. \right. \\
\left. \left. + \frac{1}{2}(p_1 + 2l_1 - P'')[2(p_2 + P_2) - (p_1 + P_1)] \right] \right\} \exp \left[\frac{i\pi}{2}(P'^2 \right. \\
\left. - P') \right] C_{[p_1+l_1],[p_2+l_2]}^* C_{\mathbf{l}}.
\end{aligned} \tag{4.4.3}$$

Here $\mathbf{q} = \mathbf{p} + \mathbf{P}$ is a reciprocal lattice vector of the Abrokosov lattice and we replaced \mathbf{ql} by \mathbf{q} .

The results of the snapshots of the diffraction pattern are shown for $a_T > t_m$ and $a_T < t_m$ in Fig. 4-4-2, respectively. I used $\langle |\Delta(\mathbf{q})|^2 \rangle$ to characterize the Bragg peaks: At $a_T = -15$, the Bragg peaks with hexagonal symmetry are separated and very sharp, indicating the existence of the triangular lattice of the vortices. But the Bragg peaks are disappeared and the diagram has a circular shape at $a_T = -8$. Thus, the most distinct difference of Bragg peaks between liquid phase and that of solid phase is the behavior of rotation symmetry. If the vortex system is in liquid state, the picture has rotation symmetry. However, the rotation symmetry will be broken while the vortex system is in solid state. Next, we calculated structure factor to obtain the melting temperature of the flux-line-lattice.



(a)



(b)

Fig. 4-4-2.

The snapshots of the diffraction pattern $\langle |\Delta(\mathbf{q})|^2 \rangle$ for (a) liquid state at $a_T = -8$ (b) solid state at $a_T = -15$. Here we set $\langle |\Delta(0)|^2 \rangle$ is neglected.

Structure factor

The definition of structure factor is

$$S(\mathbf{q}) = \chi_{DD}(\mathbf{q})/A , \quad (4.4.4)$$

A is the area of the sample. In order to discuss the phase transition between the vortex liquid and vortex lattice, I calculated the structure factor $S(\mathbf{q})$ at the maximum position $q_y = (4\pi)^{1/2}/3^{1/4}$.

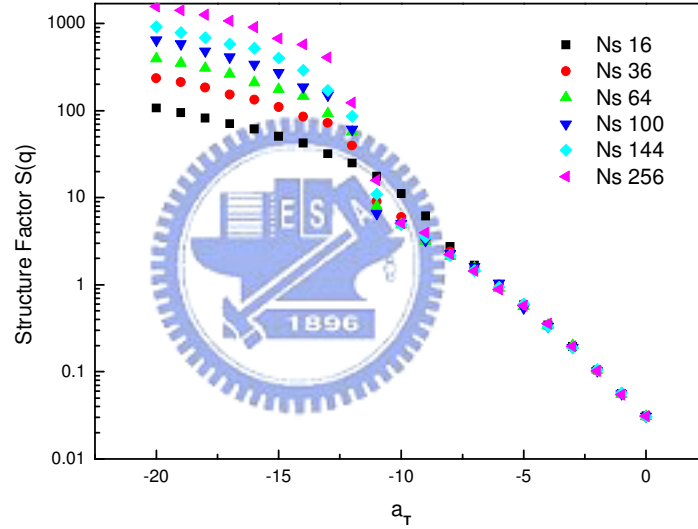


Fig. 4-4-3.

The structure factor $S(\mathbf{q})$ versus reduced temperature a_T for various system size. The squares, circles, triangles, inverted triangles, diamonds and pentangles correspond to system size $N_s = 16, 36, 64, 100, 144, 256$. Here $S(\mathbf{q})$ is in units $\frac{Tl^4}{2b}$.

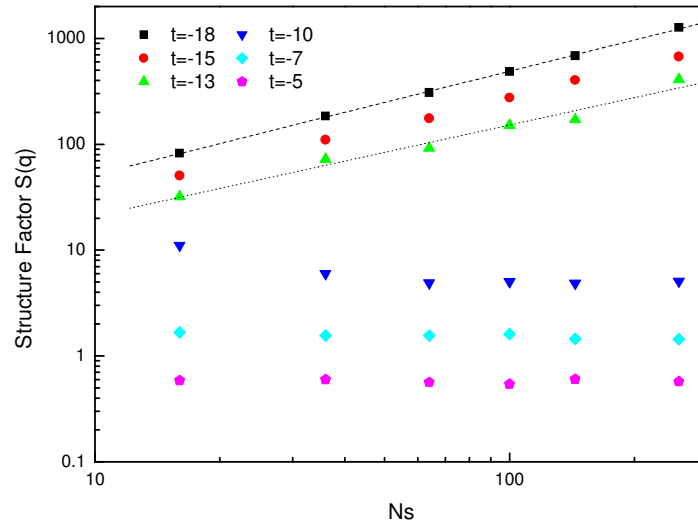


Fig. 4-4-4.

The structure factor $S(\mathbf{q})$ versus system size N_s for various reduced temperature a_T . The squares, circles, triangles, inverted triangles, diamonds and pentagles correspond to system size $a_T = -18, -15, -13, -10, -7, -5$. Here $S(\mathbf{q})$ is in units $\frac{Tl^4}{2b^i}$.



The temperature dependence of the structure factor is shown in Fig. 4-4-3. As the Monte Carlo data shows, the curves separate for $a_T < -8$ and collapse onto a single curve for $a_T > -8$. The curves splay out at $a_T = -12 \pm 2$ where indicates the transition temperature of the flux line lattice.

Furthermore, Fig. 4-4-4 shows that the size dependence of the structure. While the vortex system is in quasisoild state for $a_T < t_m$, the structure factors $S(\mathbf{q})$ are proportion to the system size N_s . However, the Monte Carlo data of structure factor $S(\mathbf{q})$ are almost constant while the vortex system is in quasi-liquid state for $a_T > t_m$. As the result, our results are close to the results of Kato and Nagaosa¹, the slope of the dotted line is approximately 0.97 and $S(\mathbf{q}) \propto N_s$, which corresponds to long-range order. The slope of

the broken line is approximately 0.85 and $S(\mathbf{q}) \propto N_s^{5/6}$, which corresponds to the size dependence at the melting point of the KTBHNY theory¹⁴⁻¹⁷.

The melting temperature for infinite vortex system size

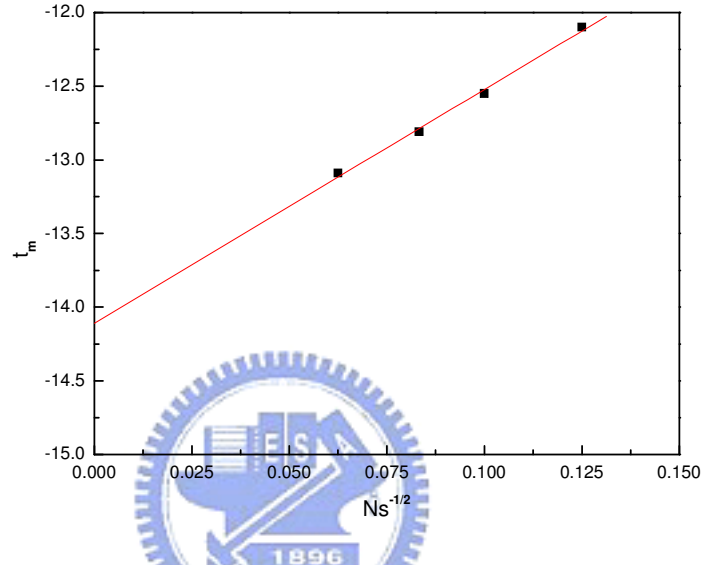


Fig. 4-4-5.

The dependence of melting temperature t_m on system size $N_s^{-1/2}$. By fitting the Monte Carlo data linearly, we found the melting temperature $t_m = -14.10932$ for the infinite system size.

Now we turn back to discuss the melting temperature for infinite vortex system size.

I provided four different system sizes, $N_s = 16^2, 12^2, 10^2, 8^2$ and the results of the size dependence of the melting temperature $t_m(N_s)$ are shown in Fig. 4-4-5. For $N_s = 16^2, 12^2, 10^2$, we find each double-peak of the internal energy distribution $P(E)$ are almost the same high. For smaller system size $N_s = 8^2$, I didn't find the double-peak in the energy distribution diagram. I determined the melting temperature of this system by at what temperature the rotation invariance was disappeared. In Fig. 3-1-10, I fitted the data by the

linear equation and found the melting temperature $t_m = -14.1 \pm 0.1$ for the infinite system size. Comparing with previous studies, $t_m = -14.3 \pm 0.2$ for $N_s \sim \infty$ by Kato and Nagaosa¹; $t_m = -13.1$ for $N_s = 144$ by Li and Nattermann³; $t_m = -13.2$ for $N_s = 12 \times 14$ by Hu and MacDonald². Thus, the melting temperature which I provided is close to the result of the previous researchers.

Chapter5 Quenched disorder

5.1 Comparison of the structure factor with that of the pure system

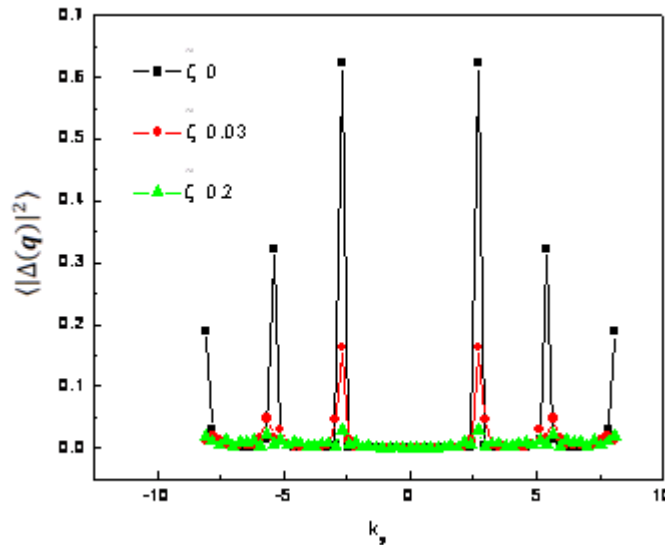
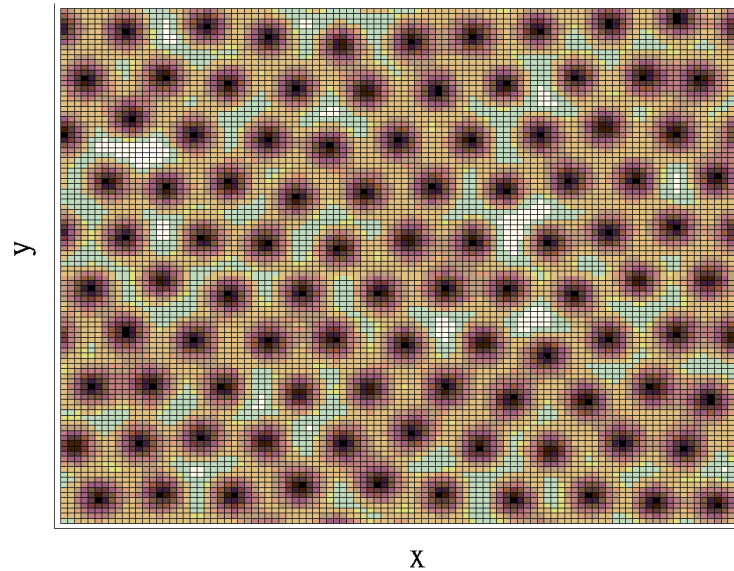


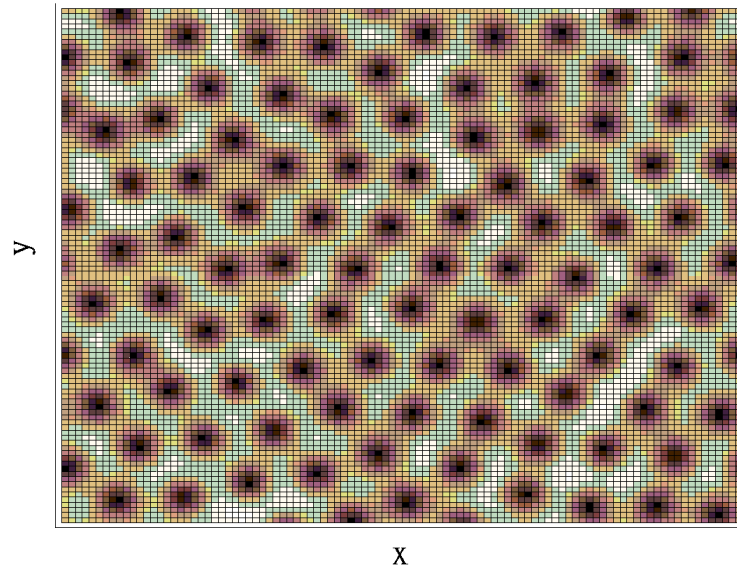
Fig. 5-1-1.

The wave vector dependence of the structure factor for disordered system at $a_T = -15$. The squares, circles and triangles correspond to $\zeta = 0$ (clean system), $\zeta = 0.03$ and $\zeta = 0.2$, respectively.

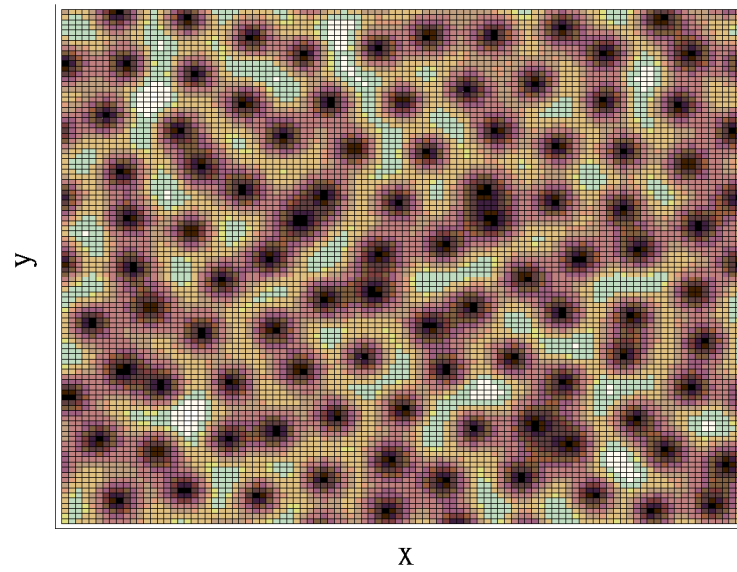
In this section, I added the disorder term to the GL free energy and discussed the difference between the clean and the disorder system. The results of k_y dependence of structure factor for three different $\tilde{\zeta}$ with $N_s = 100, a_T = -15$ are shown in Fig. 5-1-1. We took 1×10^6 Monte Carlo steps to reach equilibrium and 2×10^6 Monte Carlo steps for measure the quantity. As the result, the Bragg peaks are very sharp for $\tilde{\zeta} = 0$ case but they become shorter for $\tilde{\zeta} = 0.03$ case and $\tilde{\zeta} = 0.2$ case. Obviously, we do not find the sharp peaks for $\tilde{\zeta} = 0.2$ case. Next I discussed the snapshots of the spatial distribution of vortices position with different $\tilde{\zeta}$, the results are shown in Fig. 5-1-2. For (a) $\tilde{\zeta} = 0$ case, the system has no disorder and the configuration of vortices similar to an Abrikosov lattice. Then I applied weak disorder with (b) $\tilde{\zeta} = 0.03$ to the system and found the vortices location became slightly irregular. The configuration of vortices is more irregular as the result of (c) $\tilde{\zeta} = 0.2$ case. Thus, if we increase the value of disorder parameter $\tilde{\zeta}$, the spatial distribution of vortices position becomes more irregular.



(a)



(b)



(c)

Fig. 5-1-2.

The snapshots of the vortex position for (a) $\tilde{\zeta} = 0$ (clean system), (b) $\tilde{\zeta} = 0.03$, (c) $\tilde{\zeta} = 0.2$ with $N_s = 100$, $a_T = -15$. The range of x and y is $0 \sim L_x$ and $0 \sim L_y$ respectively and the dark spots correspond to vortex cores.

I also measured the reduced temperature dependence of structure factor for various vortex system with weak disorder $\tilde{\zeta} = 0.01$. There are six different system sizes in Fig. 5-1-3, each Monte Carlo data had been run 1×10^6 Monte Carlo steps for equilibration and 2×10^6 Monte Carlo steps for measuring the quantity. Besides, the average value was done by 80 disorder samples. As the results, the curves splay out at $a_T = -12 \pm 2$ and collapse onto a single curve for $a_T > -7$. I found the vortex system with weak disorder still has the melting transition between solid state and liquid state. It is reasonable that the melting temperature of the disorder system and that of pure system which we presented are similar since the disorder term I applied here is weak.

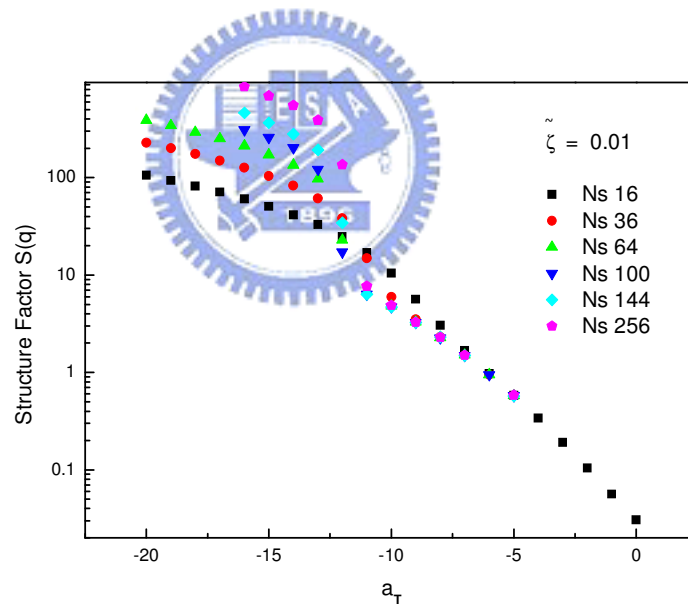


Fig. 5-1-3.

The structure factor $\overline{S(\mathbf{q})}$ in units $\frac{Tl^4}{2b'}$ versus reduce temperature a_T with $\tilde{\zeta} = 0.01$ for different system size. The squares, circles, triangles, inverted triangles, diamonds and pentangles correspond to system size $N_s = 16, 36, 64, 100, 144, 256$.

5.2 The glass line of the disorder system

In this section, I tried to find the glass line of the disorder vortex system. I introduce another disorder parameter r and glass line temperature a_T^g of the theories of B. Rosenstein and D. Li¹³. The definitions are

$$r = \frac{(1-t)^2 R'}{4\pi^2 t \xi^2 \sqrt{2Gi}}, \quad (5.2.1)$$

$$a_T^g = 2\sqrt{2} \left(\sqrt{r} - \frac{1}{\sqrt{r}} \right), \quad (5.2.2)$$

Gi is the Ginzburg number. In theory, the vortex glass become vortex liquid while $a_T > a_T^g$, see Fig. 5-2-1. If the disorder parameter r is fixed, we can obtain the corresponding value $a_T^g = c$. Hence, I simulated the disorder vortex system with fixed r and tried to find the theoretically value of a_T^g .

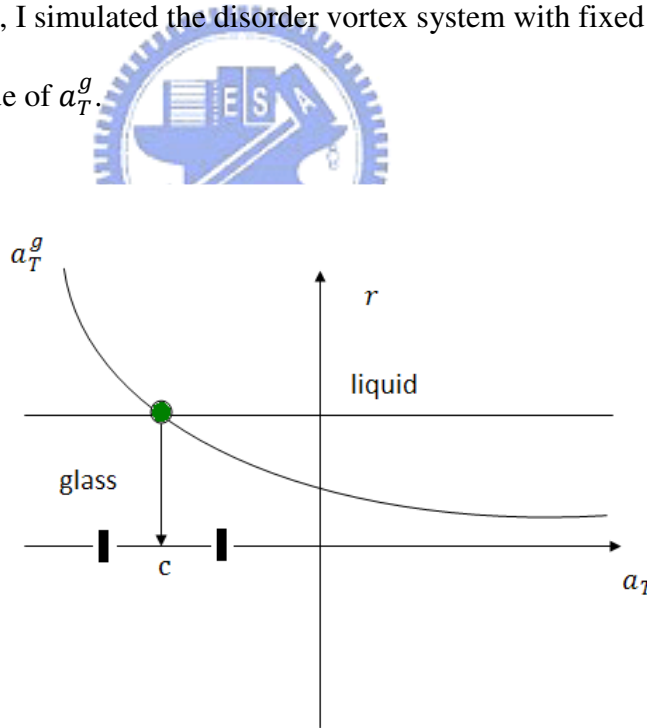


Fig. 5-2-1.
The phase diagram of vortex glass and vortex liquid which are separated by a_T^g curve

The magnetization

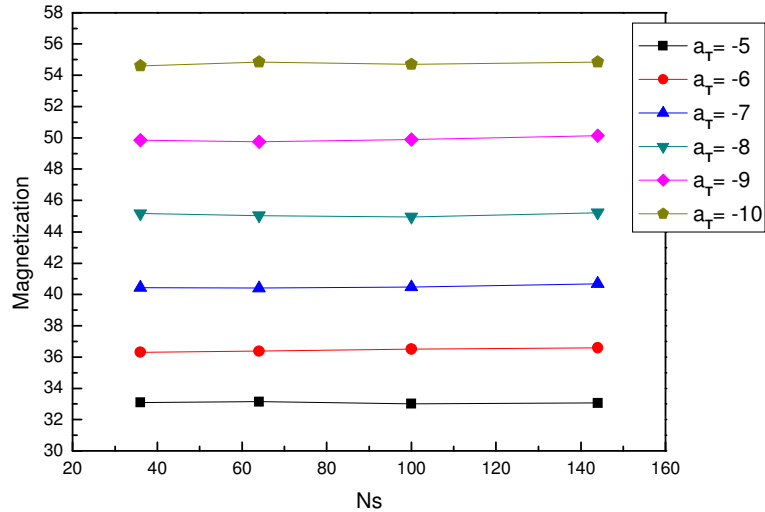


Fig. 5-2-2.

The system size dependence of magnetization for various a_T . The squares, circles, triangles, inverted triangles, diamonds and pentangles correspond to system size $a_T = -5, -6, -7, -8, -9, -10$, respectively.

The vortex systems were simulated with the disorder parameter $r = 0.32$. The Monte Carlo data had been run 1×10^6 Monte Carlo steps for equilibration and 2×10^6 Monte Carlo steps for measuring the quantity. The statistics and averages were done by 80 disorder samples. Fig. 5-2-2 shows the system size dependence of magnetization for various a_T ($-5, -6, -7, -8, -9, -10$). As the results, the disorder average of the magnetization converges very fast with the system size. The physical quantities don't depend on the system size, so that my calculation is meaningful.

The second moments

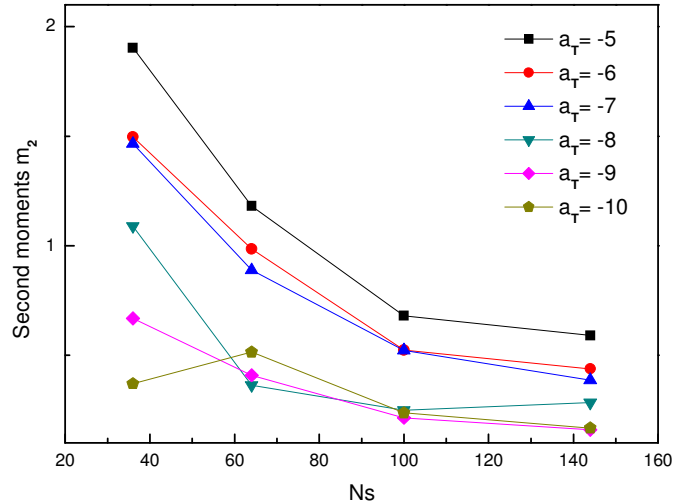


Fig. 5-2-3.

The system size dependence of second moments for various a_T . The squares, circles, triangles, inverted triangles, diamonds and pentangles correspond to system size $a_T = -5, -6, -7, -8, -9, -10$, respectively.

The results of the system size dependence of second moments for various a_T are shown in Fig. 5-2-3. As the result, the curves decay as the system size increases. In the theory, the second moments converge to a finite value in the vortex glass state; however, the second moments converge to zero in the vortex liquid state. Here I set the disorder parameter $r = 0.32$ and $a_T^g \sim -8$ theoretically. In Fig. 5-2-3, the second moments don't seem to converge to a finite value in this range of the reduce temperature. Thus, I did not find the glass line in my Monte Carlo simulation results. The detail values of other moments and the magnetization for various a_T are shown in Table 5-2-1.

Table 5-2-1

The Monte Carlo data of the nth moments and magnetization for various reduced temperature a_T .

Ns=36	2th	4th	6th	$\overline{\langle \int_r \psi(r) ^2 \rangle} / N_s$
-5.000000	1.903627	0.968647	0.785916	33.101730
-6.000000	1.496095	0.981333	0.892610	36.307093
-7.000000	1.465578	1.162532	1.412543	40.434934
-8.000000	1.089013	0.759833	0.472182	45.165741
-9.000000	0.668829	0.850774	0.602358	49.849915
-10.000000	0.369992	1.161049	1.184144	54.602529

Ns=64	2th	4th	6th	$\overline{\langle \int_r \psi(r) ^2 \rangle} / N_s$
-5.000000	1.181913	1.720579	3.088818	33.150994
-6.000000	0.985165	0.801090	0.487614	36.375821
-7.000000	0.888345	0.895439	0.695364	40.407829
-8.000000	0.363408	1.167023	1.046770	45.035289
-9.000000	0.409480	0.766420	0.508653	49.753961
-10.000000	0.514633	1.354023	1.499346	54.862039

Ns=100	2th	4th	6th	$\overline{\langle \int_r \psi(r) ^2 \rangle} / N_s$
-5.000000	0.680257	0.942989	0.748037	33.006740
-6.000000	0.523575	0.804231	0.579638	36.496617
-7.000000	0.522493	0.745477	0.418757	40.465406
-8.000000	0.249057	1.048304	0.979836	44.953665
-9.000000	0.215101	0.875568	0.593321	49.882716
-10.000000	0.237399	0.796513	0.490476	54.705229

Ns=144	2th	4th	6th	$\overline{\langle \int_r \psi(r) ^2 \rangle} / N_s$
-5.000000	0.590747	0.921689	0.832652	33.065012
-6.000000	0.437729	1.067987	1.070969	36.591659
-7.000000	0.387085	1.045748	0.974747	40.675267
-8.000000	0.283228	0.772528	0.522839	45.222984
-9.000000	0.159739	1.181599	1.227355	50.131457
-10.000000	0.167486	1.089205	1.051271	54.852637

Chapter 6 Conclusion

I have studied in this thesis certain properties of idealized 2D type II superconductor by Monte Carlo simulation in the quasimomentum basis. The vortex system is analyzed by calculation the Abrikosov ratio, specific heat, internal energy, structure factor and the phase diagram. Furthermore, I demonstrated the qualitative difference between the clean and disorder system by the vortices position and the structure factor. In clean case, as the reduce temperature increases, the values of Abrikosov ratio drop and at certain value a_T jumps indicating the first order melting transition. The data of normalized specific heat for various N_s contain a single curve unless $a_T \sim t_m$. Near the melting transition, the thermal fluctuations destroy the Abrikosov lattice, the system situation lead to liquid state. In the momentum space, the pattern shows the property of rotation symmetry while $a_T > t_m$. The Bragg peaks indicating the existence of the triangular lattice of the vortices while $a_T < t_m$. The melting transition of the vortex system is weakly first order by the double-peak of the energy distribution was found. For the infinite scale, I found the melting temperature $t_m = -14.1 \pm 0.1$, this value has a good agreement with the results of previous researchers. The curves splay out in $S(k) - a_T$ diagram, indicating that the melting temperature $t_m = -12 \pm 2$ for six system sizes ($N_s = 4 \times 4, 6 \times 6, 8 \times 8, 10 \times 10, 12 \times 12, 16 \times 16$). The data of structure factor $S(k)$ for various N_s are converged while $a_T > t_m$. However, $S(k)$ has algebraic system size dependence while $a_T < t_m$ with exponent consistent with the KTHBNY theory value of $5/6$. This is first time the whole range of quantities has been measured on the same system.

In disorder case, I added the random potential with white noise correlator to the vortex system. The disorder parameter $\tilde{\zeta}$ controls the relative disorder strength and I simulated mild disorder $\tilde{\zeta} = 0.01$ and a stronger disorder $\tilde{\zeta} = 0.03$. Abrikosov lattice is destroyed and the Bragg peaks become shorter, while the vortices are pinned by disorder. I measured distribution of magnetization using up to 80 disorder configurations. Disorder average of magnetization converges very fast with the system size, while variance and higher moments decrease. The melting line at small disorder changes insignificantly. For larger disorder, I tried to find the glass line of the disorder system with fixed material disorder parameter r . The higher moments were calculated by 40 disorder samples, the second moments of my results for scaled temperatures down to $a_T = -10$ don't show convergence to a finite value characteristic of the vortex glass. I conclude that the glass line is at lower temperatures, not accessible to MC simulation at this stage.



Appendix

Appendix A

The quadratic term of GL function is

$$\rho(x, y) = |\psi(x, y)|^2 = \sum_{k,l} C_k^* C_l \varphi_k^* \varphi_l, \quad (\text{A.1})$$

we substitute the form of the quasi-momentum

$$\varphi_k = \exp\{-ixk_x\} \varphi_0(x - k_y, y + k_x), \quad (\text{A.2})$$

into the basic formula as

$$\begin{aligned} \varphi(r) \varphi_k^*(r) = & \sum_{Q_1 \tilde{d}_1 + Q_2 \tilde{d}_2} \exp[i(\mathbf{k} + \mathbf{Q}) \cdot \mathbf{r}] \exp\left[\frac{\pi i}{2}(Q_1^2 + Q_2^2)\right] \exp\left[-\frac{(\mathbf{k} + \mathbf{Q})^2}{4}\right. \\ & \left. - \frac{i(k_x + Q_x)(k_y + Q_y)}{2} + ik_x(k_y + Q_y)\right]. \end{aligned} \quad (\text{A.3})$$

Thus, we have

$$\begin{aligned} & \varphi_0(x, y) \varphi_0^*(x - k_y, y + k_x) \\ & = \exp\{-ixk_x\} \sum_{Q_1 \tilde{d}_1 + Q_2 \tilde{d}_2} \exp[i(k_x + Q_x)x \\ & \quad + i(k_y + Q_y)y] \exp\left[\frac{\pi i}{2}(Q_1^2 + Q_2^2)\right] \exp\left[-\frac{(\mathbf{k} + \mathbf{Q})^2}{4}\right. \\ & \quad \left. - \frac{i(k_x + Q_x)(k_y + Q_y)}{2} + ik_x(k_y + Q_y)\right]. \end{aligned} \quad (\text{A.4})$$

We can rewrite Eq.(A.1) by using Eq.(A.2)

$$\begin{aligned}
\rho(x, y) &= \sum_{k,l} C_k^* C_l \varphi_k^* \varphi_l \\
&= \sum_{k,l} C_k^* C_l \exp\{ix(k_x - l_x)\} \varphi_0^*(x - k_y, y + k_x) \varphi_0(x - l_y, y + l_x).
\end{aligned}
\tag{A.5}$$

The two function product is

$$\varphi_0(x - l_y, y + l_x) \varphi_0^*(x - k_y, y + k_x),$$

set $x' = x - l_y, y' = y + l_x$

and then

$$\varphi_0(x', y') \varphi_0^*(x' - (k_y - l_y), y' + (k_x - l_x)),$$

set $k_x' = k_x - l_x, k_y' = k_y - l_y$, we have

$$\begin{aligned}
&\varphi_0(x', y') \varphi_0^*(x' - k_y', y' + k_x') \\
&= \exp\{-ix'k_x'\} \sum_Q \exp[i(k_x' + Q_x)x' \\
&\quad + i(k_y' + Q_y)y'] \exp\left[\frac{\pi i}{2}(Q_1^2 + Q_1)\right] \exp\left[-\frac{(\mathbf{k}' + \mathbf{Q})^2}{4}\right. \\
&\quad \left. - \frac{i(k_x' + Q_x)(k_y' + Q_y)}{2} + ik_x'(k_y' + Q_y)\right],
\end{aligned}$$

rewrite x', y' by x, y and k_x', k_y' by k_x, k_y

$$\begin{aligned}
& \varphi_0(x - l_y, y + l_x) \varphi_0^*(x - k_y, y + k_x) \\
&= \exp\{-i(x - l_y)(k_x - l_x)\} \sum_{\mathbf{Q}} \exp[i(k_x - l_x + Q_x)(x - l_y) \\
&+ i(k_y - l_y + Q_y)(y + l_x)] \exp\left[\frac{\pi i}{2}(Q_1^2 + Q_1)\right] \exp\left[-\frac{(\mathbf{k} - \mathbf{l} + \mathbf{Q})^2}{4}\right. \\
&\left. - \frac{i(k_x - l_x + Q_x)(k_y - l_y + Q_y)}{2} + i(k_x - l_x)(k_y - l_y + Q_y)\right]
\end{aligned} \tag{A.6}$$

substituting Eq.(A.6) into Eq.(A.3)

$$\begin{aligned}
\rho(x, y) &= \sum_{\mathbf{k}, \mathbf{l}} C_{\mathbf{k}}^* C_{\mathbf{l}} \exp\{ix(k_x - l_x)\} \varphi_0^*(x - k_y, y + k_x) \varphi_0(x - l_y, y + l_x) \\
&= \sum_{\mathbf{k}, \mathbf{l}} \sum_{\mathbf{Q}} \exp\{ix(k_x - l_x)\} \exp\{-i(x - l_y)(k_x - l_x)\} \exp[i(k_x - l_x + Q_x)(x - l_y) \\
&+ i(k_y - l_y + Q_y)(y + l_x)] \exp\left[\frac{\pi i}{2}(Q_1^2 + Q_1)\right] \exp\left[-\frac{(\mathbf{k} - \mathbf{l} + \mathbf{Q})^2}{4}\right. \\
&\left. - \frac{i(k_x - l_x + Q_x)(k_y - l_y + Q_y)}{2} + i(k_x - l_x)(k_y - l_y + Q_y)\right] C_{\mathbf{k}}^* C_{\mathbf{l}} \\
&= \sum_{\mathbf{k}, \mathbf{l}} \sum_{\mathbf{Q}} \exp\{il_y(k_x - l_x)\} \exp[i(k_x - l_x + Q_x)x - i(k_x - l_x + Q_x)l_y \\
&+ i(k_y - l_y + Q_y)y \\
&+ i(k_y - l_y + Q_y)l_x] \exp\left[\frac{\pi i}{2}(Q_1^2 + Q_1)\right] \exp\left[-\frac{(\mathbf{k} - \mathbf{l} + \mathbf{Q})^2}{4}\right. \\
&\left. - \frac{i(k_x - l_x + Q_x)(k_y - l_y + Q_y)}{2} + i(k_x - l_x)(k_y - l_y + Q_y)\right] C_{\mathbf{k}}^* C_{\mathbf{l}}
\end{aligned}$$

$$\begin{aligned}
&= \sum_{k,l} \sum_{\mathbf{Q}} \exp\{il_y(k_x - l_x)\} \exp[i(k_x - l_x + Q_x)x - i(k_x - l_x + Q_x)l_y \\
&\quad + i(k_y - l_y + Q_y)y] \exp\left[\frac{\pi i}{2}(Q_1^2 + Q_1)\right] \exp\left[-\frac{(\mathbf{k} - \mathbf{l} + \mathbf{Q})^2}{4}\right. \\
&\quad \left. - \frac{i(k_x - l_x + Q_x)(k_y - l_y + Q_y)}{2} + ik_x(k_y - l_y + Q_y)\right] C_{\mathbf{k}}^* C_{\mathbf{l}}.
\end{aligned} \tag{A.7}$$

Appendix B

We start from the equation of $|\psi(x, y)|^2$

$$\begin{aligned}
\rho(x, y) &= \sum_{k,l} \sum_{\mathbf{Q}} \exp\{il_y(k_x - l_x)\} \exp[i(k_x - l_x + Q_x)x + i(k_y - l_y + Q_y)y \\
&\quad - i(k_x - l_x + Q_x)l_y] \exp\left[\frac{i\pi}{2}(Q_1^2 - Q_1)\right] \exp\left[-\frac{(\mathbf{k} - \mathbf{l} + \mathbf{Q})^2}{4}\right. \\
&\quad \left. - \frac{i(k_x - l_x + Q_x)(k_y - l_y + Q_y)}{2} + ik_x(k_y - l_y + Q_y)\right] C_{\mathbf{k}}^* C_{\mathbf{l}},
\end{aligned} \tag{B.1}$$

and the Fourier transform of $\rho(x, y)$ is

$$\begin{aligned}
\tilde{\rho}(\mathbf{x}, \mathbf{y}) &= \frac{1}{2\pi L^2} \int dx dy \exp[-i(\mathbf{p} + \mathbf{P}) \\
&\quad \cdot \mathbf{r}] \sum_{k,l} \sum_{\mathbf{Q}} \exp\{il_y(k_x - l_x)\} \exp[i(k_x - l_x + Q_x)x + i(k_y - l_y + Q_y)y \\
&\quad - i(k_x - l_x + Q_x)l_y] \exp\left[\frac{i\pi}{2}(Q_1^2 - Q_1)\right] \exp\left[-\frac{(\mathbf{k} - \mathbf{l} + \mathbf{Q})^2}{4}\right. \\
&\quad \left. - \frac{i(k_x - l_x + Q_x)(k_y - l_y + Q_y)}{2} + ik_x(k_y - l_y + Q_y)\right] C_{\mathbf{k}}^* C_{\mathbf{l}}.
\end{aligned}$$

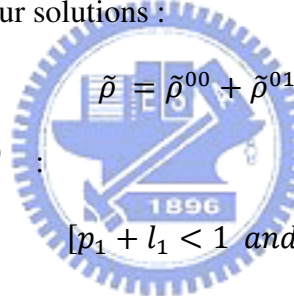
(B.2)

Integration over x and y

$$\begin{aligned}
\tilde{\rho}(\mathbf{p} + \mathbf{P}) = & \sum_{\mathbf{k}, \mathbf{l}} \sum_{\mathbf{Q}} \delta[\mathbf{p} + \mathbf{P} - (\mathbf{k} - \mathbf{l} + \mathbf{Q})] \exp\{il_y(k_x - l_x)\} \exp[i(k_x - l_x + Q_x)x \\
& + i(k_y - l_y + Q_y)y - i(k_x - l_x + Q_x)l_y] \exp\left[\frac{i\pi}{2}(Q_1^2 \right. \\
& \left. - Q_1)\right] \exp\left[-\frac{(\mathbf{k} - \mathbf{l} + \mathbf{Q})^2}{4} - \frac{i(k_x - l_x + Q_x)(k_y - l_y + Q_y)}{2}\right. \\
& \left. + ik_x(k_y - l_y + Q_y)\right] C_{\mathbf{k}}^* C_{\mathbf{l}}.
\end{aligned}$$

(B.3)

The Kronecker delta has four solutions :



$$\tilde{\rho} = \tilde{\rho}^{00} + \tilde{\rho}^{01} + \tilde{\rho}^{10} + \tilde{\rho}^{11}. \quad (\text{B.4})$$

(B.4)

1. Major contribution $\tilde{\rho}^{00}$:

$$[p_1 + l_1 < 1 \text{ and } p_2 + l_2 < 1]$$

$$Q_1 = P_1; k_1 = p_1 + l_1; Q_2 = P_2; k_2 = p_2 + l_2$$

(B.5)

Substitute (B.5) into (B.3)

$$\begin{aligned}
\tilde{\rho}^{00}(\mathbf{p} + \mathbf{P}) = & \sum_{\mathbf{l}} \exp\left\{i\pi\left[-P_1(2l_2 - l_1) \right. \right. \\
& \left. \left. + \frac{1}{2}(p_1 + 2l_1 - P_1)[2(p_2 + P_2) - (p_1 + P_1)]\right]\right\} \exp\left[\frac{i\pi}{2}(P_1^2 \right. \\
& \left. - P_1)\right] \exp\left[-\frac{(\mathbf{p} + \mathbf{P})^2}{4}\right] C_{p_1+l_1, p_2+l_2}^* C_{\mathbf{l}}.
\end{aligned}$$

(B.6)

2. One umklapp contribution $\tilde{\rho}^{01}$:

$$[p_1 + l_1 > 1 \text{ and } p_2 + l_2 < 1]$$

$$Q_1 = P_1 + 1; k_1 = p_1 + l_1 - 1; Q_2 = P_2; k_2 = p_2 + l_2$$

(B.7)

Substitute (B.7) into (B.3)

$$\begin{aligned} \tilde{\rho}^{01}(\mathbf{p} + \mathbf{P}) = & \sum_l \exp \left\{ i\pi \left[-(P_1 + 1)(2l_2 - l_1) \right. \right. \\ & \left. \left. + \frac{1}{2}(p_1 + 2l_1 - P_1 - 2)[2(p_2 + P_2) - (p_1 + P_1)] \right] \right\} \exp \left\{ \frac{i\pi}{2} [(P_1 + 1)^2 \right. \\ & \left. - (P_1 + 1)] \right\} \exp \left[-\frac{(\mathbf{p} + \mathbf{P})^2}{4} \right] C_{p_1+l_1-1, p_2+l_2}^* C_l. \end{aligned}$$

(B.8)

3. One umklapp contribution



$\tilde{\rho}^{10}$:

$$[p_1 + l_1 < 1 \text{ and } p_2 + l_2 > 1]$$

$$Q_1 = P_1; k_1 = p_1 + l_1; Q_2 = P_2 + 1; k_2 = p_2 + l_2 - 1$$

(B.9)

Substitute (B.10) into (B.3)

$$\begin{aligned} \tilde{\rho}^{10}(\mathbf{p} + \mathbf{P}) = & \sum_l \exp \left\{ i\pi \left[-P_1(2l_2 - l_1) \right. \right. \\ & \left. \left. + \frac{1}{2}(p_1 + 2l_1 - P_1)[2(p_2 + P_2) - (p_1 + P_1)] \right] \right\} \exp \left[\frac{i\pi}{2} (P_1^2 \right. \\ & \left. - P_1) \right] \exp \left[-\frac{(\mathbf{p} + \mathbf{P})^2}{4} \right] C_{p_1+l_1, p_2+l_2-1}^* C_l. \end{aligned}$$

(B.10)

4. The two umklapp contribution $\tilde{\rho}^{11}$:

$$[p_1 + l_1 > 1 \text{ and } p_2 + l_2 > 1]$$

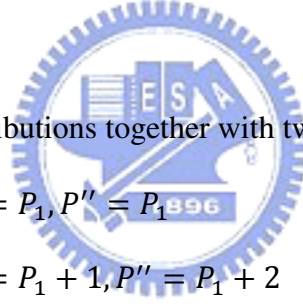
$$Q_1 = P_1 + 1; k_1 = p_1 + l_1 - 1; Q_2 = P_2 + 1; k_2 = p_2 + l_2 - 1$$

(B.11)

Substitute (B.11) into (B.3)

$$\begin{aligned} \tilde{\rho}^{11}(\mathbf{p} + \mathbf{P}) = \sum_l \exp \left\{ i\pi \left[-(P_1 + 1)(2l_2 - l_1) \right. \right. \\ \left. \left. + \frac{1}{2}(p_1 + 2l_1 - P_1 - 2)[2(p_2 + P_2) - (p_1 + P_1)] \right] \right\} \exp \left\{ \frac{i\pi}{2} [(P_1 + 1)^2 \right. \\ \left. - (P_1 + 1)] \right\} \exp \left[-\frac{(\mathbf{p} + \mathbf{P})^2}{4} \right] C_{p_1+l_1-1, p_2+l_2-1}^* C_l. \end{aligned}$$

(B.12)



Finally, we putted all contributions together with two conditions :

1. *if* $(p_1 + l_1) < 1 \rightarrow P' = P_1, P'' = P_1$
2. *if* $(p_1 + l_1) > 1 \rightarrow P' = P_1 + 1, P'' = P_1 + 2$

and we obtain

$$\begin{aligned} \tilde{\rho}(\mathbf{p} + \mathbf{P}) = \sum_l \exp \left\{ i\pi \left[-P'(2l_2 - l_1) \right. \right. \\ \left. \left. + \frac{1}{2}(p_1 + 2l_1 - P'')[2(p_2 + P_2) - (p_1 + P_1)] \right] \right\} \exp \left[\frac{i\pi}{2} (P'^2 \right. \\ \left. - P') \right] \exp \left[-\frac{(\mathbf{p} + \mathbf{P})^2}{4} \right] C_{[p_1+l_1], [p_2+l_2]}^* C_l. \end{aligned}$$

(B.13)

here $C_{[p_1+l_1]}$ indicates $C_{(p_1+l_1 \bmod L)}$.

Appendix C

The energy of new configuration can be calculated by using

$$C_{l_1, l_2}^{new} = C_{l_1, l_2}^{old} + \delta_{l_1 - j_1} \delta_{l_2 - j_2} \Delta \quad (C.1)$$

Hence, the new superfluid density term is

$$\begin{aligned} \int_{x,y}^{new} |\Psi(x, y)|^2 &= 2\pi L^2 \sum_{l_1, l_2} C_{l_1, l_2}^{new*} C_{l_1, l_2}^{new} \\ &= 2\pi L^2 \sum_{l_1, l_2} (C_{l_1, l_2} C_{l_1, l_2}^{old} + \delta_{l_1 - j_1} \delta_{l_2 - j_2} \Delta)^* (C_{l_1, l_2}^{old} + \delta_{l_1 - j_1} \delta_{l_2 - j_2} \Delta) \\ &= 2\pi L^2 \sum_{l_1, l_2} (C_{l_1, l_2}^{old} C_{l_1, l_2}^{old*} + C_{j_1, j_2}^{old*} \Delta + C_{j_1, j_2}^{old} \Delta^* + \Delta \Delta^*) \\ &= \int_{x,y}^{old} |\Psi(x, y)|^2 + 2\pi L^2 (C_{j_1, j_2}^{old*} \Delta + C_{j_1, j_2}^{old} \Delta^* + \Delta \Delta^*). \end{aligned} \quad (C.2)$$

According to Eq.(2.2.14) and Eq.(2.3.9), we can obtain the new interaction term and disorder term by calculating $\tilde{\rho}(\mathbf{p} + \mathbf{P})$, so that

$$\begin{aligned} \tilde{\rho}(\mathbf{p} + \mathbf{P}) &= \sum_l \exp \left\{ i\pi \left[-P'(2l_2 - l_1) \right. \right. \\ &\quad \left. \left. + \frac{1}{2} (p_1 + 2l_1 - P'') [2(p_2 + P_2) - (p_1 + P_1)] \right] \right\} \exp \left[\frac{i\pi}{2} (P'^2 \right. \\ &\quad \left. - P') \right] \exp \left[-\frac{(\mathbf{p} + \mathbf{P})^2}{4} \right] (C_{[p_1+l_1], [p_2+l_2]}^{old*} + \delta_{[p_1+l_1]-j_1} \delta_{[p_2+l_2]-j_2} \Delta^*) (C_{l_1, l_2}^{old} \\ &\quad + \delta_{l_1 - j_1} \delta_{l_2 - j_2} \Delta). \end{aligned} \quad (C.3)$$

This calculation result can be separated into four part for different delta function solutions

as follows

(a)

$$\sum_l \exp \left\{ i\pi \left[-P'(2l_2 - l_1) + \frac{1}{2}(p_1 + 2l_1 - P'')[2(p_2 + P_2) - (p_1 + P_1)] \right] \right\} \exp \left[\frac{i\pi}{2}(P'^2 - P') \right] \exp \left[-\frac{(\mathbf{p} + \mathbf{P})^2}{4} \right] (C_{[p_1+l_1],[p_2+l_2]}^{old*} C_{l_1,l_2}^{old}). \quad (C.4)$$

(b)

$$\begin{aligned} & \sum_l \exp \left\{ i\pi \left[-P'(2l_2 - l_1) + \frac{1}{2}(p_1 + 2l_1 - P'')[2(p_2 + P_2) - (p_1 + P_1)] \right] \right\} \exp \left[\frac{i\pi}{2}(P'^2 - P') \right] \exp \left[-\frac{(\mathbf{p} + \mathbf{P})^2}{4} \right] (\delta_{[p_1+l_1]-j_1} \delta_{[p_2+l_2]-j_2} \Delta^* C_{l_1,l_2}^{old}) \\ &= \exp \left\{ i\pi \left[-P'(2[j_2 - p_2] - [j_1 - p_1]) + \frac{1}{2}(p_1 + 2[j_1 - p_1] - P'')[2(p_2 + P_2) - (p_1 + P_1)] \right] \right\} \exp \left[\frac{i\pi}{2}(P'^2 - P') \right] \exp \left[-\frac{(\mathbf{p} + \mathbf{P})^2}{4} \right] (C_{[j_1-p_1],[j_2-p_2]}^{old} \Delta^*). \end{aligned} \quad (C.5)$$

(c)

$$\begin{aligned} \tilde{\rho}(\mathbf{p} + \mathbf{P}) &= \sum_l \exp \left\{ i\pi \left[-P'(2l_2 - l_1) + \frac{1}{2}(p_1 + 2l_1 - P'')[2(p_2 + P_2) - (p_1 + P_1)] \right] \right\} \exp \left[\frac{i\pi}{2}(P'^2 - P') \right] \exp \left[-\frac{(\mathbf{p} + \mathbf{P})^2}{4} \right] (C_{[p_1+l_1],[p_2+l_2]}^{old*} \delta_{l_1-j_1} \delta_{l_2-j_2} \Delta) \end{aligned}$$

$$\begin{aligned}
&= \exp \left\{ i\pi \left[-P'(2j_2 - j_1) + \frac{1}{2}(p_1 + 2j_1 - P'')[2(p_2 + P_2) - (p_1 + P_1)] \right] \right\} \exp \left[\frac{i\pi}{2}(P'^2 \right. \\
&\quad \left. - P') \right] \exp \left[-\frac{(\mathbf{p} + \mathbf{P})^2}{4} \right] (C_{[p_1+j_1],[p_2+j_2]}^{old*} \Delta).
\end{aligned} \tag{C.6}$$

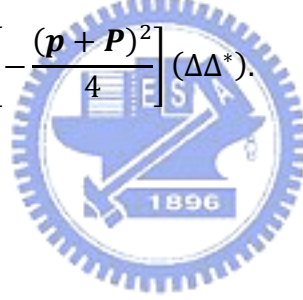
(d)

$$\begin{aligned}
&\sum_l \exp \left\{ i\pi \left[-P'(2l_2 - l_1) + \frac{1}{2}(p_1 + 2l_1 - P'')[2(p_2 + P_2) - (p_1 + P_1)] \right] \right\} \exp \left[\frac{i\pi}{2}(P'^2 \right. \\
&\quad \left. - P') \right] \exp \left[-\frac{(\mathbf{p} + \mathbf{P})^2}{4} \right] (\delta_{[p_1+l_1]-j_1} \delta_{[p_2+l_2]-j_2} \delta_{l_1-j_1} \delta_{l_2-j_2} \Delta \Delta^*) \\
&= \exp \left\{ i\pi \left[-P'(2j_2 - j_1) + \frac{1}{2}(2j_1 - P'')[2(P_2) - (P_1)] \right] \right\} \exp \left[\frac{i\pi}{2}(P'^2 \right. \\
&\quad \left. - P') \right] \exp \left[-\frac{(\mathbf{p} + \mathbf{P})^2}{4} \right] (\Delta \Delta^*).
\end{aligned} \tag{C.7}$$

Finally, we substitute Eq.(C.4) ~ Eq.(C.7) into Eq.(C.3)

$$\begin{aligned}
\tilde{\rho}(\mathbf{p} + \mathbf{P}) &= \sum_l \exp \left\{ i\pi \left[-P'(2l_2 - l_1) \right. \right. \\
&\quad \left. \left. + \frac{1}{2}(p_1 + 2l_1 - P'')[2(p_2 + P_2) - (p_1 + P_1)] \right] \right\} \exp \left[\frac{i\pi}{2}(P'^2 \right. \\
&\quad \left. - P') \right] \exp \left[-\frac{(\mathbf{p} + \mathbf{P})^2}{4} \right] (C_{[p_1+l_1],[p_2+l_2]}^{old*} C_{l_1,l_2}^{old})
\end{aligned}$$

$$\begin{aligned}
& + \exp \left\{ i\pi \left[-P'(2j_2 - p_2) - [j_1 - p_1] \right. \right. \\
& \quad \left. \left. + \frac{1}{2}(p_1 + 2[j_1 - p_1] - P'')[2(p_2 + P_2) - (p_1 + P_1)] \right] \right\} \exp \left[\frac{i\pi}{2} (P'^2 \right. \\
& \quad \left. - P') \right] \exp \left[-\frac{(\mathbf{p} + \mathbf{P})^2}{4} \right] (C_{[j_1 - p_1], [j_2 - p_2]}^{old} \Delta^*) \\
& + \exp \left\{ i\pi \left[-P'(2j_2 - j_1) + \frac{1}{2}(p_1 + 2j_1 - P'')[2(p_2 + P_2) - (p_1 + P_1)] \right] \right\} \exp \left[\frac{i\pi}{2} (P'^2 \right. \\
& \quad \left. - P') \right] \exp \left[-\frac{(\mathbf{p} + \mathbf{P})^2}{4} \right] (C_{[p_1 + j_1], [p_2 + j_2]}^{old*} \Delta) \\
& + \exp \left\{ i\pi \left[-P'(2j_2 - j_1) + \frac{1}{2}(2j_1 - P'')[2(P_2) - (P_1)] \right] \right\} \exp \left[\frac{i\pi}{2} (P'^2 \right. \\
& \quad \left. - P') \right] \exp \left[-\frac{(\mathbf{p} + \mathbf{P})^2}{4} \right] (\Delta \Delta^*).
\end{aligned}$$



(C.8)

References

- ¹ Y. Kato and N. Nagaosa, Phys. Rev. B **47**, 2932 (1993); **48**,7383 (1993).
- ² J. Hu and A.H. MacDonald, Phys. Rev. Lett. **71**, 432 (1993).
- ³ M. S. Li and T. Natterman, Phys. Rev. B. **67**, 194520 (2003).
- ⁴ A. A. Abrikosov, Zh. Eksp. Teor. Fiz. **32**,1444 (1957).
- ⁵ J. A. O'Neill and M. A. Moore, Phys. Rev. B. **48**, 374 (1992).
- ⁶ A. K. Kienappel and M. A. Moore, Phys. Rev. B. **60**, 6795 (1999).
- ⁷ H. H. Lee and M. A. Moore, Phys. Rev. B. **49**, 9240 (1994).
- ⁸ J. Hu and A. H. MacDonald, Phys. Rev. B. **49**, 15263 (1994).
- ⁹ J. Hu and A. H. MacDonald, Phys. Rev. B. **56**, 2788 (1997).
- ¹⁰ M. J. Dodgson and M. A. Moore, Phys. Rev. B. **55**, 3816 (1997).
- ¹¹ R. Sasik and D. Stroud, Phys. Rev. B. **49**, 16074 (1994).
- ¹² D. Li and B. Rosenstein, Phys. Rev. B. **60**, 9704 (1999).
- ¹³ D. Li, B. Rosenstein and V. Vinokur, Journal of superconductivity and Novel Magnetism. **19**, 369 (2006).

- ¹⁴ J. M. Kosterlitz and D. J. Thouless, J. Phys. Phs. C 6, 1881 (1973).
- ¹⁵ B. I. Halperin and D. R. nelson, Phys. Rev. Lett. 41, 121(1978).
- ¹⁶ D. R. nelson and B. I. Halperin, Phys. Rev. B19, 2457(1979).
- ¹⁷ A. P. Young, Phys. Rev. B19, 1855(1979).
- ¹⁸ B. Rosenstein and D. Li. The Ginzburg-Landau Theory of Type II superconductors. 2007. (Unpublished).
- ¹⁹ J. B. Ketterson and S. N. Song. Superconductivity. Cambridge, 1999.
- ²⁰ C. P. Poole, H. A. Farach and R. J. Creswick. Superconductivity. Academic Press, 1995.
- ²¹ D. P. Landau and K. Binder. Monte Carlo simulations in Statistical Physics. Cambridge, 2000.
- ²² 陳思， “Monte Carlo simulation of vortex-line melting in type-II two-dimensional superconductors” ， 北京大學， 2005。